# STUDY ON BISMUTH OXYIODIDE FOR PHOTOVOLTAIC CELL APPLICATION

太陽電池応用のためのビスマス酸ヨウ化物に関する研究

**ANISSA ADIWENA PUTRI**

**NAGOYA INSTITUTE OF TECHNOLOGY**

**2020**

## TABLE OF CONTENT

**Chapter 7**

# CHAPTER 1

# INTRODUCTION

## 1.1. Photovoltaic cell

The demand of nanostructured metal oxide materials usage has increased significantly over the past decade since those materials are known to have wide application [1]. For the photovoltaic application, some metal oxide nanomaterials have been developed to be a component in the device. The common material which has been studied mostly so far in photovoltaic device is titanium dioxide ($TiO_2$) since it performs the enormous ability for energy conversion from solar energy to electricity energy [2,3]. $TiO_2$ application for photovoltaic device has become greater after O'Regan and Grätzel introduced the utilized of $TiO_2$ for photoanode in solar cell system sensitized with dye which is known as dye-sensitized solar cell (DSSC) in 1991 [2]. Since then, solar cell research based on this model can be considered as an interesting topic until nowadays because of its environmentally friendly character and it employs renewable resources.

Many researchers have modified the composition in the photovoltaic cell and designed the cell arrangement as the effort to increase the photovoltaic performance. One of the important parts which can be considered as the major component is photoanode. This part is the most studied component in photovoltaic cell development. It can act as good photoanode if it has good transparency and excellent contact with the visible light. To build a good photoanode, some experiments were reported, like the physical modification on the $TiO_2$ and ZnO photoanodes by post-annealing treatment [4–7] and the doping treatment to the semiconductor materials with inorganic and organic material [8,9]. By those modifications, it had the impact on the electrical

transport properties in photoanode and resulted in a better performance than undoped material and non-composite films [10,11].

In photovoltaic solar cell device, there is one component which has the ability to harvest the light for transporting the charge carrier, namely absorber material. Silicon (Si) is the most solar absorber used which can perform the solar efficiency for more than 20%. Nowadays, silicon solar cell has been commercializing as the photovoltaic material because it has been considered as the reasonable-cost material which has good reliability to live longer [12]. However, to apply silicon for photovoltaic application, it needs higher purity silicon. In other words, silicon is low-defect tolerance material.

Besides Si, some inorganic materials have been produced for solar cell purposes, for instance $Cu(In,Ga)Se_2$/ CIGS and CdTe materials. Recently, the new material which based on the organic and inorganic material and adapted the perovskite structure, $ABX_3$, namely $CH_3NH_3PbI_3$ (methyl ammonium lead idodide/ MAPI) has attracted the attention among researchers due to its good performance. The solar efficiency comes from MAPI is competitive to the silicon solar cell and it can be a great solution for finding an alternative to get the higher efficiency from solar cell device which has increased from 3 to 22.1% during this 10 years [13,14]. Also, MAPI can be considered as the high tolerance in defect which no need the high level in its purity for photovoltaic application. As the consequence, low cost in synthesis of this material can be a good thing for mass production of MAPI in this application.

A rapid rising in the solar cell of lead-halide perovskite caused the use of it has been preferred and most developed in recent years. However, behind the use of lead perovskite, it remains problems to the environment [15]. Lead is known as the toxic material which is dangerous for human living although it performs a competitive performance in comparison to the

silicon. The risk of lead contained in material will not only danger to the human and living beings, but it is also dangerous to the environment [16]. Therefore, many researchers have tried to find another way for replacing Pb in the perovskite structure. The second problem in the Pb-perovskite application is its instability. Generally, it is known that Pb-perovskite with the structure $MAPbI_3$ is easy to be decomposed due to the humidity, UV light, and high temperature [17–20]. Some efforts have been attempted to improve the stability of this layer, for example, device encapsulation [21,22], using the stable electrode which is compatible to the perovskite [23,24], and hydrophobic polymer incorporation [25–27].

Since Pb has the ns2 valence electron, it can be replaced with Bi which sits next to Pb in the periodic table. Bi also can be categorized as a heavy metal but it has low toxicity than Pb. Based on this fact, Bi can be attempted to be an alternative of lead [28]. Bismuth(III) is isoelectronic to Pb(II) and it tends to be more stable than Tin(II). Therefore, so many reports informed the use of $Bi^{3+}$ in the perovskite structure instead of $Pb^{2+}$ to obtain the more environmental benign solar cell structure [29–31] although the efficiency is still on the enhancement process [32]. Moreover, another bismuth-based material namely bismuth oxyiodide (BiOI) can be considered as the promising material for photovoltaic materials and it will be studied on this work.

## 1.2. Inorganic photovoltaic cell

The crystalline and amorphous inorganic compounds, like silicon (Si), CdTe, chalcopyrite compound, copper indium gallium diselenide (CIGS) have been utilized as the component in the photovoltaic device. Beside those materials, hybrid-perovskite solar cells have demonstrated a tremendous potential component in solar cell structure which has been indicated by the great performance of this material. Single and polycrystalline silicon, gallium arsenide (GaAs), and cadmium telluride (CdTe) are also being the most popular inorganic photovoltaic device. In

inorganic photovoltaic cells, the semiconducting element is purposed for light absorption. Generally, it contains a p-n junction consists of a p-type and an n-type semiconductor, which are involved as the hole and electron transport layer.

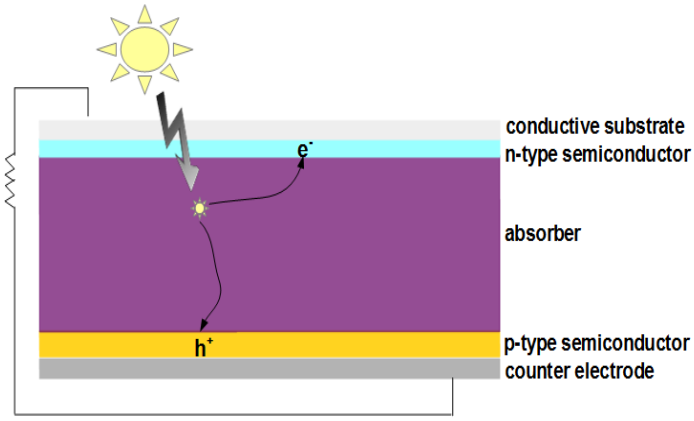


**Fig. 1.1** Structure of common inorganic solar cell.

The illustration which is shown in Fig. 1.1 is the common composition in the inorganic solar cell. It contains the conductive substrate, an n-type semiconductor, absorber, p-type semiconductor, and counter electrode (metal electrode). When the absorber absorbs the suitable radiation, the photon can hit the electron to flow across the p-n junction which resulted in the electricity due to the photoelectric effect. Commercial Si is the most popular material for inorganic photovoltaic cell because of its good stability and high power conversion efficiency. However, to purify silicon still needs cost. Hence, it needs alternate materials which are cheap, high defect tolerance and environmental benign with a competitive performance.

## 1.3. Absorber in photovoltaic cell

Absorber can be considered as the main component in the solar cell device since this part can harvest the light, absorb it and result in the charge carrier transport within the electrical device. The most common solar cell absorber is thick polycrystalline silicon (Si) which performs high

efficiency for more than 20%. Other absorbers have been developed based on the inorganic materials, like CdTe and CIGS. However, CdTe and CIGS are toxic. Another absorber in PV technology is $CH_3NH_3PbI_3$, Pb-perovskite which is cheap and can result in the higher efficiency of solar cell. However the used of Pb in the MAPI structure can be harmful for human living.

## 1.4. Bismuth oxyiodide (BiOI)

Bismuth-based compound is the Pb-free material which is easy to synthesis, has the lower toxicity in comparison to among semiconductor materials [33–35] and high tolerance in defect [36]. Generally, bismuth-based materials can be synthesized by some routes, like sonochemical method, hydrothermal method, and chemical bath deposition. Materials composed with bismuth can be categorized as the p-type semiconductor. As it has good activity under the visible spectral range, it is suitable in the application for photocatalyst, absorber in photovoltaic cell, and water purification [37–40]. The hybridized valence between 6s in Bi(III) and 2p in oxygen causes the bismuth-based materials become active in the visible range. Hence, the bismuth oxyhalide, BiOX (X = Cl, Br, I) can perform the excellent optical and electrical properties which make it will be promising for various application, especially in photocatalysis.

Bismuth oxyiodide (BiOI) can be classified as the V-VI-VII semiconductor materials with matlockite structure and slabbed structure consisting of [X-Bi-O-Bi-X] layer by van der Walls interaction through the halogen atom. BiOX has the covalent bond in all atoms within the layer and it also causes the excellent mechanical and optical properties. Moreover, bismuth atom has the asymmetric decahedral symmetry which is constructed by four oxygen and halogen atoms. For the structure of BiOI, it is depicted in the Figure 1.2.

Among the BiOCl and BiOF, BiOI has the narrower band gap energy which is around 1.59 eV with band edge absorption at 645 nm. The calculation of band gap follows the indirect band

gap and it has been informed that the contribution of 2p in oxygen and np states in halides has the impact on the maximum level in conduction band. Also, the 6p states in bismuth atom flavors the conduction band minimum level since the covalent bond strength in Bi-O > Bi-I [42].

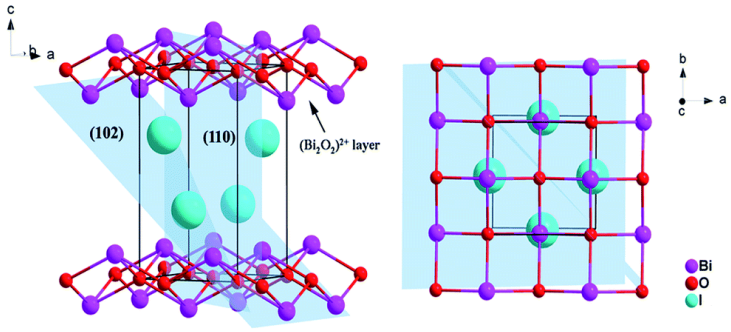


**Fig. 1.2** Structure of BiOI [41].

## 1.5. BiOI for absorber material in photovoltaic device

BiOI can act as the material for solar cell with low cost and low toxicity. At the beginning, the BiOI utilization for photovoltaic material was adapted from DSSC-like arrangement. For the first time, Zhao *et al* prepared the solar cell based on the BiOI by mixing BiOI nanoplate with the chitosan material (CHI). BiOI-CHI performed the Voc which was only 0.461 V and Jsc was 20.4 $\mu A/cm^2$ [43]. Later, Wang and co-workers developed the solar cell based on BiOI with the crossed flake-like arrays through the successive ionic layer absorption and reaction (SILAR) method to synthesize BiOI. By using this method and involving the Pt-counter electrode with iodine electrolyte, 0.092% of efficiency and ~6.5% of IPCE value could be obtained without utilizing any n-type semiconductor [44,45].

For a better improvement in BiOI solar cell, Zhang *et al* and Sfaelou *et al* tried to use BiOI for replacing the dye in DSSC. They made the cell with arrangement: $TiO_2$/BiOI/Iodine electrolyte/Pt-counter electrode. The difference in both works is the way of BiOI synthesis method. Zhang *et al* developed BiOI by the CBD method, while Sfaelou *et al* used SILAR

method. By CBD, the maximum cell efficiency was 0.38% and surprisingly, 1.03% of efficiency could be obtained in the Sfaelou and team's [46,47]. However, it is interesting to note that in those works, the thicker BiOI used in the substrate lowered the solar cell performance. The bigger size of BiOI after the more cycles by CBD caused the ineffective contact between BiOI as p-type and $TiO_2$ as n-type semiconductor. Furthermore, the $TiO_2$ quality seems also to be the crucial impact on the BiOI solar cell performance.

Later, Hoye and co-worker developed the solar cell based on the bismuth material which had the highest efficiency so far (~1.7%) by using the suitable hole and electron transport layer, namely NiOx and ZnO. In that work, the solar cell construction contained the pure inorganic materials, ITO/NiOx/BiOI/ZnO/Al with the air ambient stability up to 197 days [36]. In addition, Zhang and team combined the usage of BiOI and $Fe_2O_3$ as the photoanode in photovoltaic device. In that work, 0.55% as the maximum of efficiency performance could be obtained and it has been proven that BiOI can be mixed with other materials which showed the performance enhancement in comparison to its single material [48]. Thus, it is considered that BiOI is easy to prepare, low cost in preparation, having a good activity under the visible light and fascinating stability, and it has environmentally friendly character which make BiOI is still worth to be developed and studied.

## 1.6. Challenge in BiOI solar cell

Although the limit efficiency performance of BiOI is still low, it has been reported to have a better stability and low toxicity. It also has been mentioned that BiOI can be a promising material for photovoltaic cell since it has a life time which up to 2.7 ns [36]. BiOI still can show the photovoltaic properties although the result is far away from other materials. However, due to

the BiOI stability and its environmentally friendly, it is important to complete BiOI solar cell study by developing and preparing BiOI with different way.

Referring to the application of BiOX materials for photocatalyst aspect, it has been noticed that the physical properties of this material, like crystal phase, dimension, shape, and size affect much on the photocatalytic behavior. The different synthesis method may result in the different synthesized material properties which can result in the different dimension, for example 1-D, 2-D, 3-D, and other hollow nanostructures. Those materials can give the different light absorption ability [49]. As the consequence, the ability to contact with the UV-Visible light may change. This behavior also has the influence on the material for photovoltaic device. Here, this thesis proposed the way for synthesizing BiOI materials and studying its effect on the photovoltaic devices. Moreover, BiOI with smaller size is required to improve the BiOI performance in solar cell since the recombination probability in the photogenerated charges might be enhanced due to the BiOI overdeposition.

## 1.7. Research objective

To develop BiOI application for photovoltaic device, the more study on BiOI can be carried out by trying to synthesize BiOI in other ways. It is supposed that by different method and treatment in BiOI synthesis, it results in the different properties which is interesting and may have the different compositions and morphological structures. Therefore, it will result in the different photovoltaic performance. This thesis described how to prepare BiOI by a modified SILAR and changing the angle position during the dip coating work, exploring the different precursor concentration, developing BiOI films through spin-coating which involved the SILAR process (spin-SILAR), and applying the annealing treatment on the prepared BiOI powder. In

addition, application of less-iodide bismuth material which can act as the photocatalyst, namely $Bi_5O_7I$ for photovoltaic device application is also discussed.

## 1.8. References

[1] M. Bilgili, H. Bilirgen, A. Ozbek, F. Ekinci, T. Demirdelen, *Renew. Energy* 126 (2018) 755–764.

[2] B. O'Regan, M. Grätzel, *Nature* 353 (1991) 737–740.

[3] A. Hagfeldt, B. Didriksson, T. Palmqvist, H. Lindström, S. Södergren, H. Rensmo, S.-E. Lindquist, *Sol. Energy Mater. Sol. Cells* 31 (1994) 481–488.

[4] M.S.H. Choudhury, N. Kishi, T. Soga, *Jpn. J. Appl. Phys.* 55 (2016) 01AE13.

[5] M.S.H. Choudhury, N. Kishi, T. Soga, *Jpn. J. Appl. Phys.* 55 (2016) 01AA16.

[6] M.S.H. Choudhury, N. Kishi, T. Soga, *2017 IEEE 44th Photovolt. Spec. Conf. PVSC 2017* (2017) 1–6.

[7] M.S. Haque Choudhury, N. Kishi, T. Soga, *Mater. Res. Bull.* 80 (2016) 135–138.

[8] Z. Xu, X. Yin, Y. Guo, Y. Pu, M. He, *J. Mater. Chem. C* 6 (2018) 4746–4752.

[9] S. Li, L. Chen, K. Zhang, S. Wu, X. Shen, J. Zhao, *Org. Electron.* 59 (2018) 1–6.

[10] M.S.H. Choudhury, S. Kato, N. Kishi, T. Soga, *Jpn. J. Appl. Phys.* 56 (2017) 04CS05.

[11] A.A. Abuelwafa, M.S.H. Choudhury, M. Dongol, M.M. El-Nahass, T. Soga, *J. Mater. Sci. Mater. Electron.* 29 (2018) 14232–14238.

[12] M. Yamaguchi, K.H. Lee, K. Araki, N. Kojima, *J. Phys. D. Appl. Phys.* 51 (2018) 133002.

[13] A. Kojima, K. Teshima, Y. Shirai, T. Miyasaka, *J. Am. Chem. Soc.* 131 (2009) 6050–6051.

[14] W.S. Yang, B.-W. Park, E.H. Jung, N.J. Jeon, Y.C. Kim, D.U. Lee, S.S. Shin, J. Seo, E.K. Kim, J.H. Noh, S. Il Seok, *Science* 356 (2017) 1376–1379.

[15] W. Tan, A.R. Bowring, A.C. Meng, M.D. McGehee, P.C. McIntyre, *ACS Appl. Mater. Interfaces* 10 (2018) 5485–5491.

[16] A. Babayigit, A. Ethirajan, M. Muller, B. Conings, *Nat. Mater.* 15 (2016) 247–251.

[17] G. Niu, X. Guo, L. Wang, *J. Mater. Chem. A* 3 (2015) 8970–8980.

[18] G. Abdelmageed, L. Jewell, K. Hellier, L. Seymour, B. Luo, F. Bridges, J.Z. Zhang, S. Carter, *Appl. Phys. Lett.* 109 (2016) 233905.

[19] H. Zhou, C. Qi, L. Gang, L. Song, S. Tze-bing, D. Hsin-Sheng, H. Ziruo, J. You, L. Yongsheng, Y. Yan, *Science (80-. ).* 345 (2014) 542–546.

[20] J. Yang, B.D. Siempelkamp, D. Liu, T.L. Kelly, *ACS Nano* 9 (2015) 1955–1963.

[21] S. Guarnera, A. Abate, W. Zhang, J.M. Foster, G. Richardson, A. Petrozza, H.J. Snaith, *J. Phys. Chem. Lett.* 6 (2015) 432–437.

[22] Q. Dong, F. Liu, M.K. Wong, H.W. Tam, A.B. Djurišić, A. Ng, C. Surya, W.K. Chan, A.M.C. Ng, *ChemSusChem* 9 (2016) 2597–2603.

[23] J. Zhao, X. Zheng, Y. Deng, T. Li, Y. Shao, A. Gruverman, J. Shield, J. Huang, *Energy Environ. Sci.* 9 (2016) 3650–3656.

[24] Z. Liu, B. Sun, T. Shi, Z. Tang, G. Liao, *J. Mater. Chem. A* 4 (2016) 10700–10709.

[25] S.N. Habisreutinger, T. Leijtens, G.E. Eperon, S.D. Stranks, R.J. Nicholas, H.J. Snaith, *Nano Lett.* 14 (2014) 5561–5568.

[26] X. Li, M. Ibrahim Dar, C. Yi, J. Luo, M. Tschumi, S.M. Zakeeruddin, M.K. Nazeeruddin, H. Han, M. Grätzel, *Nat. Chem.* 7 (2015) 703–711.

[27] F. Bella, G. Griffini, J.-P. Correa-Baena, G. Saracco, M. Grätzel, A. Hagfeldt, S. Turri, C. Gerbaldi, *Science* 354 (2016) 203–206.

[28] A.A.A. Khan, M.A. Abdullah, *Int. J. Electrochem. Sci.* 8 (2013) 195–203.

[29] B.-W. Park, B. Philippe, X. Zhang, H. Rensmo, G. Boschloo, E.M.J. Johansson, *Adv. Mater.* 27 (2015) 6806–6813.

[30] M. Leng, Z. Chen, Y. Yang, Z. Li, K. Zeng, K. Li, G. Niu, Y. He, Q. Zhou, J. Tang, *Angew. Chemie Int. Ed.* 55 (2016) 15012–15016.

[31] F. Giustino, H.J. Snaith, *ACS Energy Lett.* 1 (2016) 1233–1240.

[32] S.M. Jain, T. Edvinsson, J.R. Durrant, *Commun. Chem.* 2 (2019) 91.

[33] L.M. Fraas, Y. Ma, *J. Cryst. Growth* 39 (1977) 92–107.

[34] A. Munshi, W. Sampath, *J. Electron. Mater.* 45 (2016) 4612–4619.

[35] Q. Zhang, F. Hao, J. Li, Y. Zhou, Y. Wei, H. Lin, *Sci. Technol. Adv. Mater.* 19 (2018) 425–442.

[36] R.L.Z. Hoye, L.C. Lee, R.C. Kurchin, T.N. Huq, K.H.L. Zhang, M. Sponseller, L. Nienhaus, R.E. Brandt, J. Jean, J.A. Polizzotti, A. Kursumović, M.G. Bawendi, V. Bulović, V. Stevanović, T. Buonassisi, J.L. MacManus-Driscoll, *Adv. Mater.* 29 (2017) 1–10.

[37] W.F. Yao, X.H. Xu, H. Wang, J.T. Zhou, X.N. Yang, Y. Zhang, S.X. Shang, B.B. Huang, *Appl. Catal. B Environ.* 52 (2004) 109–116.

[38] H. Cheng, B. Huang, K. Yang, Z. Wang, X. Qin, X. Zhang, Y. Dai, *ChemPhysChem* 11 (2010) 2167–2173.

[39] H. Cheng, B. Huang, J. Lu, Z. Wang, B. Xu, X. Qin, X. Zhang, Y. Dai, *Phys. Chem. Chem. Phys* 12 (2010) 15468–15475.

[40] X. Lin, S.S. Jiang, Z. Lin, M. Wang, Y.S. Yan, *IOP Conf. Ser. Mater. Sci. Eng.* 137 (2016) 012020.

[41] H. Huang, K. Liu, Y. Zhang, K. Chen, Y. Zhang, N. Tian, *RSC Adv.* 4 (2014) 49386–

49394.

[42] L. Zhao, X. Zhang, C. Fan, Z. Liang, P. Han, *Phys. B Condens. Matter* 407 (2012) 3364–3370.

[43] K. Zhao, X. Zhang, L. Zhang, *Electrochem. Commun.* 11 (2009) 612–615.

[44] K. Wang, F. Jia, Z. Zheng, L. Zhang, *Electrochem. Commun.* 12 (2010) 1764–1767.

[45] K. Wang, F. Jia, L. Zhang, *Mater. Lett.* 92 (2013) 354–357.

[46] Y. Zhang, Q. Pei, J. Liang, T. Feng, X. Zhou, H. Mao, W. Zhang, Y. Hisaeda, X.M. Song, *Langmuir* 31 (2015) 10279–10284.

[47] S. Sfaelou, D. Raptis, V. Dracopoulos, P. Lianos, *RSC Adv.* 5 (2015) 95813–95816.

[48] Y. Zhang, Y. Li, W. Sun, C. Yuan, B. Wang, W. Zhang, X.M. Song, *Langmuir* 33 (2017) 12065–12071.

[49] F.E. Osterloh, *Chem. Soc. Rev.* 42 (2013) 2294–2320.

# CHAPTER 2

# DIFFERENT ANGLE EFFECT ON THE PREPARED BiOI BY DIP-COATING METHOD FOR PHOTOVOLTAIC APPLICATION

## 2.1. Introduction

BiOI which is p-type semiconductor can be used as one of parts for solar cell device. However, the efficiency is still low. Therefore, it is important to optimize the short-circuit current density (Jsc) and open-circuit voltage (Voc) of BiOI solar cell. The effort to increase the efficiency of BiOI solar cell can be carried out by modifying the way to synthesis BiOI. Due to the different method and applying some different treatment in the material synthesis route, the different properties of materials will come and it may effect on its application.

Some methods are common to obtain BiOI which can be applied for inorganic sensitizer in photovoltaic devices and photocatalyst [1,2]. First, the conventional method which involved the solvent usage has been developed by Zhang and co-workers for BiOI synthesis and application for photocatalyst, namely solvothermal method. Next, Wang and co-workers prepared BiOI by successive ionic layer adsorption and reaction (SILAR). By this method, flakes array of BiOI/$TiO_2$ composite could be applied for solar cell device for the first time. It resulted in the Jsc at 0.23 mA/$cm^2$ [16]. Another work for BiOI solar cell by SILAR with $TiO_2$ layer resulted in the Jsc for 3.8 mA/$cm^2$ [5]. By using SILAR also, it resulted in BiOI solar cell for Jsc around 0.529 mA/$cm^2$ [6]. The work which is nearly same as SILAR is chemical bath deposition (CBD) which could reveal the performance for BiOI/$TiO_2$ solar cell with the Jsc was 1.5 mA/$cm^2$ [14]. Both SILAR and CBD are highlighted to be the common methods in BiOI preparation for solar cell application. By those methods, it is known that the film thickness is depended on the number of cycles during the SILAR and CBD methods.

Thickness in the prepared films by dip-coating may be controlled by the lifting speed during the coating process [7], fluid concentration [7], viscosity [8], and the angle during the withdrawal on the dip-coating [9–12]. Especially by involving the angle variation in dip coating, the thickness layer can be modified on the upper and the opposite side of substrate [13]. The equation in Eq. 2.1 shows that the characteristic scale of film thickness ($h_0$) depends on the $u_w$ value which is the function of lifting speed from the liquid chamber, angle ($\theta$), and the fluid properties, such as constant density ($\rho$) and viscosity ($\mu$). By involving an angle inclination while dip coating process, it resulted in the thicker layer on the upper side with the different angle from $90^o$ to $30^o$ [9,14].

$$h_0 = \left(\frac{\mu u_w}{\rho g \sin\theta}\right)^{1/2} \quad (2.1)$$

Since the study on the effect of angle inclination for BiOI preparation by SILAR is not reported yet, this chapter describes how to fabricate BiOI films and studied the angle impact on the prepared films and its photovoltaic properties by adapting the work from previous report [6]. The different angle resulted in the different properties of BiOI films which may come from the different thickness, size, and morphology of BiOI films. Furthermore, each photovoltaic property of prepared material by the different angle in dip-coating will be not similar. This result is expected to support the evidence that the angle inclination for material preparation also has the effect on the material properties which impacts on the ability of BiOI absorption in the visible light spectral range which is important for solar cell application.

## 2.2. Synthesis and fabrication of BiOI films

The modified SILAR with the different substrate angle during the dip-coating process which adapted from Wang and co-workers' work was used for BiOI films preparation [6]. The same mole ratios of $Bi(NO_3).5H_2O$ and KI were prepared in aqueous solution. Glass/ FTO substrates

were used as the substrates with the size 2 x 2 cm. Each substrate was cleaned in acetone (twice) and ethanol (once) which was followed by $N_2$ gas blowing into the substrates before UV/$O_3$ treatment for 30 minutes in total. The angle inclination in SILAR with dip-coating is depicted in Fig. 2.1 with the angle (α) variation from 50 to 90°. After the films were obtained, the heating treatment at 100 °C was carried out.

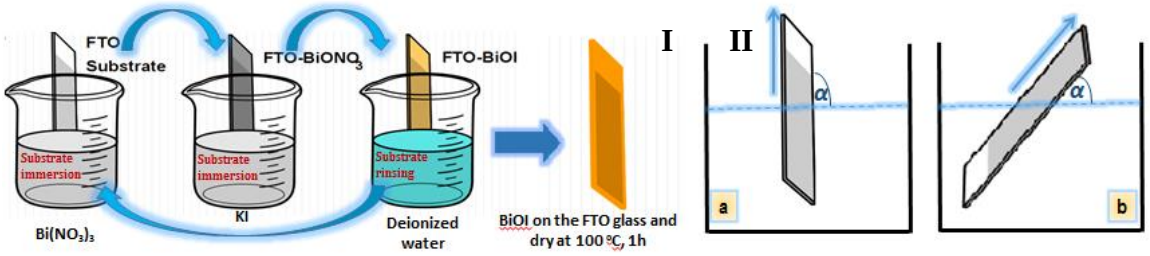


**Fig. 2.1.** BiOI deposition illustration by modified SILAR (I), vertical (α=90°) dip coating (IIa), and angled (α≠90°) dip coating (IIb).

For solar cell application, the resulted films were used as photoanode. The Pt-coated glass was utilized as the counter electrode and $I^-/I_3^-$ redox (Solaronix Iodolyte AN-50) was set up for the electrolyte liquid media. All of the samples were test with a solar simulator (100 mW/cm$^2$, AM 1.5 illumination) in the air with the area 0.16 cm$^2$. Further characterization was finished by using X-Ray diffraction (XRD, Rigaku SmartLab), Raman Spectrometer (Raman, JASCO NRS-2100), UV-Visible NIR Spectroscopy (UV-Vis NIR Spectrophotometer, JASCO 670 UV), and Field Emission Scanning Electron Microscope (FESEM, JEOL JSM-7001F).

## 2.3. Dip-coating angle effect on the structural properties of BiOI

### 2.3.1. Structural study by Raman spectra

Raman spectrophotometer was used for structural study of prepared BiOI. From the Fig. 2.2, Raman spectra shows the peak around 149.6 cm$^{-1}$ for the (Eg) vibration mode of Bi-I. This result is in line with the previous report [15]. Although there are other types of Raman active BiOI

vibrational modes, namely $A_{1g}$ and $B_{1g}$ can be found in the BiOI structure, in this work, both those modes are not existed since it could not be observable in the Raman machine like in the previous report [16]. By the angle decreasing, it is found that the intensity of BiOI peak increased. It might come from the thickening of prepared BiOI at angle $50^{o}$ in comparison to the other samples.

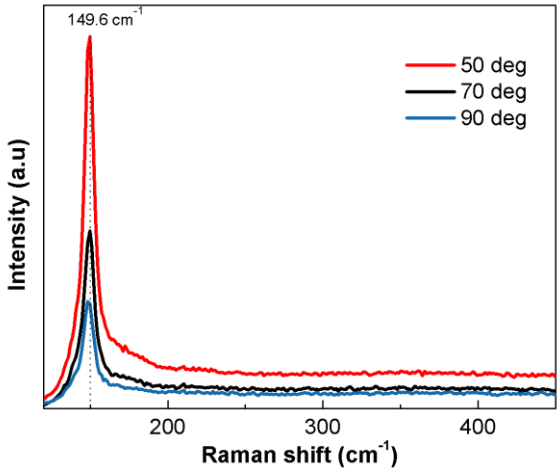


**Fig. 2.2.** Raman spectra of prepared BiOI films with varied angled dip-coating.

### 2.3.2. Crystal analysis by XRD

In the Fig. 2.3, it is showed the XRD patterns of prepared BiOI films via angled dip-coating. From the depicted patterns it is noticed that the resulted BiOI is matched to the JCPDS card no. 73-2062 for BiOI material. The attributed peaks for BiOI are 2θ $29.6^{o}$, $31.7^{o}$, and $45.5^{o}$ for (012), (110), and (020) crystal planes. There was no impurity found in the samples and those peaks were similar to the BiOI tetragonal phase pattern from the previous research [17]. Therefore, it is convinced that BiOI was successfully synthesized via this process.

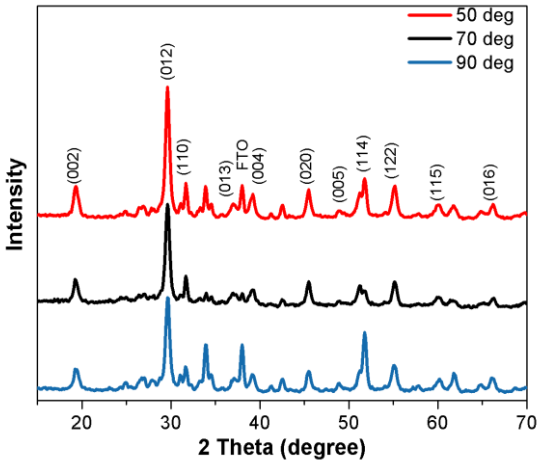


**Fig. 2.3.** XRD patterns of prepared BiOI films with varied angled dip-coating.

Crystal size calculation was carried out using Debye-Scherrer equation in Eq. 2.2 [18] (L is the size of crystal, K is constant (0.9), λ is Cu wavelength (0.154 nm), β is the FWHM in radian, and θ is the Bragg angle for the diffraction peaks). The resulted crystallite size was 21.25; 18.87; and 18.53 nm, respectively for prepared BiOI at $50^o$; $70^o$; and $90^o$. By those results, it can be seen that the different angle has a slight impact on the different material crystallite size.

$$L = \frac{K\lambda}{\beta Cos\theta} \qquad (2.2)$$

## 2.4. Optical properties of prepared BiOI

The UV-Visible spectra are displayed in the Fig. 2.4. From the transmittance data (Fig. 2.4.a), the synthesized BiOI film vertically has the less transparency than others. By reducing the angle during dip-coating, it resulted in the more orange films. This result is line with the Raman spectra. The remained BiOI in the substrates by the different angle influences the absorbance behavior (Fig. 2.4.b). The more agglomeration of BiOI might occur in the lower angle which caused the more BiOI in the substrates. As a result, the more orange and concentrated BiOI films were obtained with the wider absorption in visible region. The thickening film from the tilting

angle ranging from 90° to 50° caused the shifting of wavelength from 660 nm to 680 nm and the present study has a good agreement with the reported research [19,20].

To calculate the band gap energy, Tauc plot equation in Eq. 2.3 was used, where α, v, Eg, and A represent the coefficient of absorption, frequency of light, band gap energy, and a constant, respectively. Last, the n value can be 1 for direct transition and 4 for indirect transition [31–34].

$$\alpha hv = A\left(hv - E_g\right)^{n/2} \qquad (2.3)$$

Due to the lowering angle, it makes slight different band gap energy of BiOI, from 1.9 to 1.8 eV. Semiconductor optical properties can have a good correlation with the morphology and material size. Especially for BiOI, BiOI nanoplatelets band gap energy is lower than BiOI nanoflakes [25]. BiOI band gap energy in this experiment is close to the reported work which related to the BiOI synthesis and characterization [26–32]. Moreover, band gap energy also can be affected by the atomic distance and grain size [33].

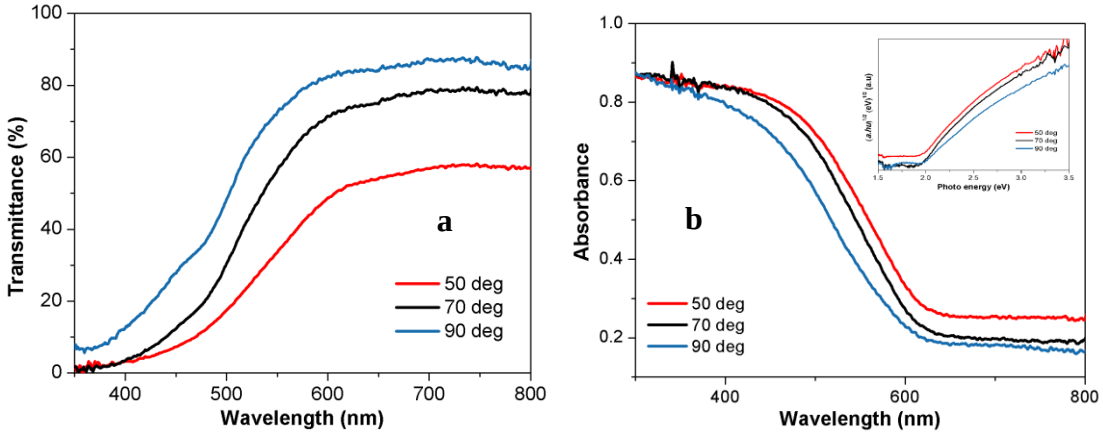


**Fig. 2.4.** UV-vis transmittance (a) and absorbance spectra (b) of synthesized BiOI films with varied angled dip-coating. Inset: Tauc plot for indirect band gap, $(\alpha hv)^{1/2}$ vs photon energy ($hv$).

## 2.5. Morphological study of prepared BiOI

Fig. 2.5 shows that the SEM images of prepared BiOI films in the different angle are the flaky BiOI. It was in line to the previous reports [3,5,6]. Based on the previous reported BiOI

experiment, it was known that 2D structure for BiOI such as flaky and plate-like structure are typically grown perpendicularly [34]. Here, it is found that in the vertical substrate, the flake morphology dominated and it had the thickness around 25 nm with the lateral size ranged in the submicron area between 100 and 300 nm (Fig. 2.5c and f). However, in the tilted angle, BiOI films had the larger size of flake which up to 800 nm. The more BiOI deposition due to the tilting substrate could result in the larger particle and the thicker BiOI films. The proposed illustration of angled substrate for BiOI preparation is shown in Fig. 2.6.

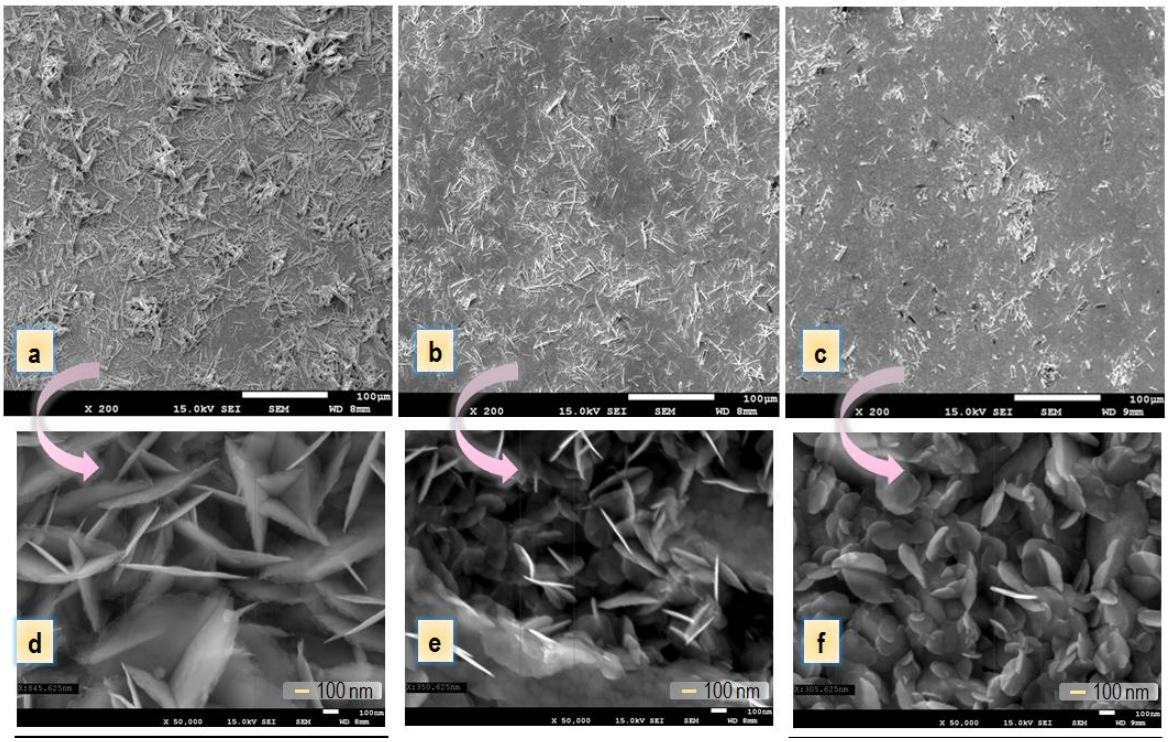


**Fig. 2.5.** SEM images of BiOI films with varied angled dip-coating $50^{o}$ (a); $70^{o}$ (b); $90^{o}$ (c), and image in the higher magnitude from prepared film at $50^{o}$ (d); $70^{o}$ (e); $90^{o}$ (f).

The lower angle orientation might allow the changing of height interface in the inclined substrate in comparison to the vertical substrate. The remained material in the inclined substrates may be more in comparison to the perpendicular sample. Therefore, the thicker BiOI will be obtained from the tilted substrates. By the film thickness analysis, the prepared sample by $50^{o}$ of

substrates had the thickness around 3 µm while the perpendicular substrates resulted in the 1 µm -thick of BiOI films. Also, the gravity effect and hydrostatic pressure might promote the more BiOI deposition in the substrates to result in the thicker films besides the reducing sin θ value based on the Eq. 2.1 [11]. Then overall, BiOI is easy to be deposited massively at lower angle. It might reduce the surface free energy and reach the crystal stability. The deposition illustration in this work is depicted in Fig. 2.6.

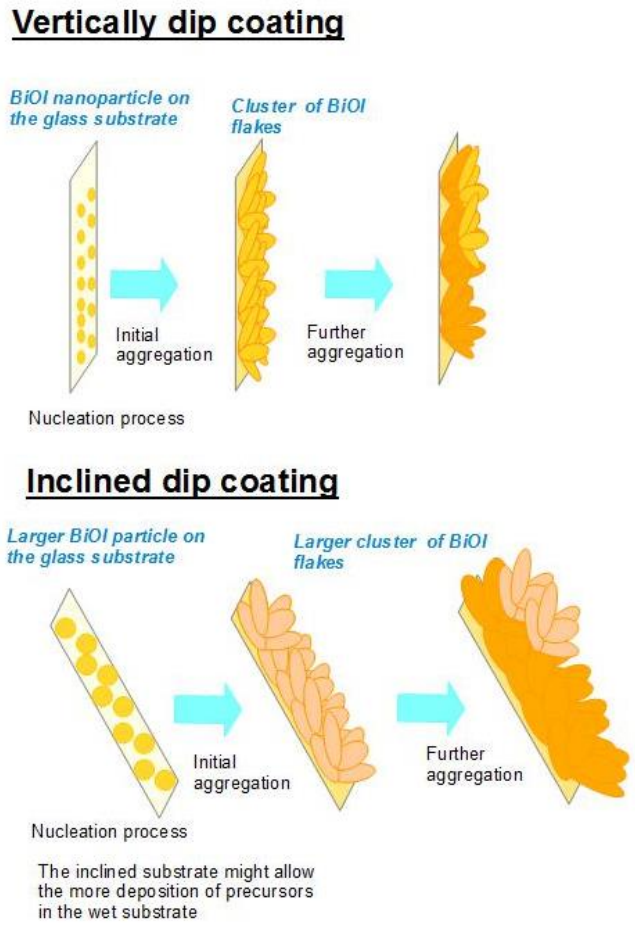


**Fig. 2.6.** Illustration of BiOI growth model in the perpendicular and tilted substrates.

## 2.6. Photovoltaic property of BiOI

Fig. 2.7a shows the IV curve of prepared BiOI films and Fig. 2.7b illustrates the solar cell construction. A maximum of short-circuit density about 1.47 mA/cm$^2$ could be obtained and it

was almost three times higher from the previous results in nanoflakes and nanoplatelets BiOI solar cell [6,34]. The open-circuit voltage was around 0.46 V. The declining photovoltaic parameters might be caused by the film thickening with the increasing in the morphology and size of BiOI.

The larger size of flake morphology might have the smaller surface area and it could reduce the active site area. The surface area of BiOI film might increase along with the higher angle, like mesoporous $TiO_2$ for dye-sensitized solar cells. The less contact between electrolyte and bigger semiconductor material might be responsible to reduce Jsc value and decrease the electron exchange in photovoltaic cell. Moreover, the morphology might affect the free charge mobility and exciton dissociation in the solar cell. Then, it could decrease the photovoltaic performance. When the band gap energy increased, a small increment of Voc also can be obtained.

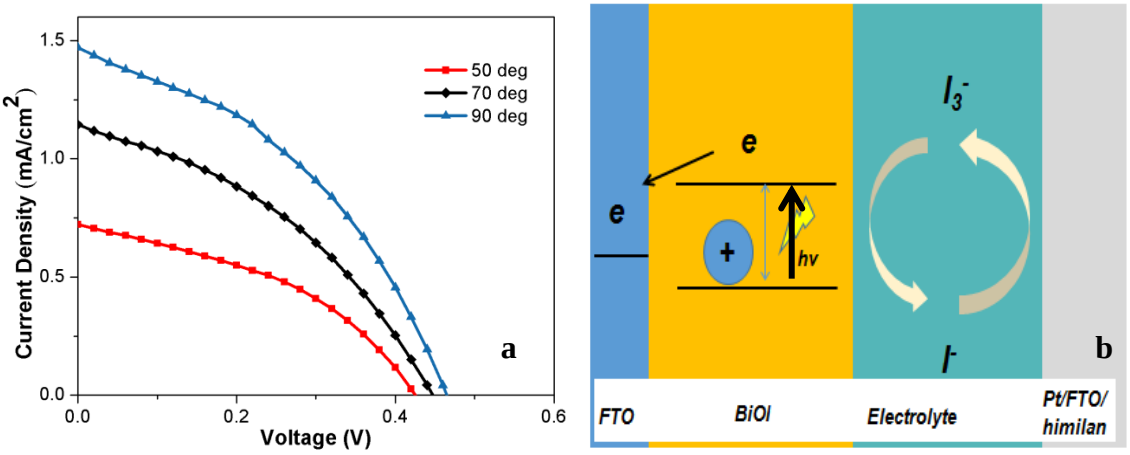


**Fig. 2.7.** I-V curves of BiOI/FTO with synthesized BiOI films with varied angled dip-coating (a) and schematic of BiOI/FTO solar cell (b).

## 2.7. Conclusions

Angle variation in the dip coating process could result in the different properties BiOI films, like the optical properties, crystallinity, size, and morphology due to the thickening layer. A smaller flake size from the vertical FTO substrate exhibited the better Jsc and Voc which up to

1.47 mA/cm$^2$ and 0.465 V. Those results were higher than those measured in the previous studies. By the research result, it could be concluded that substrate angle inclination had the effect on the resulted films by SILAR which based on the dip-coating. Furthermore, to get a better performance of BiOI films for solar cell, a further optimization in BiOI preparation is needed to get the more controlled BiOI morphology.

## 2.8. References


[1] X. Zhang, L. Zhang, T. Xie, D. Wang, *J. Phys. Chem. C* 113 (2009) 7371–7378.

[2] L. Wang, W.A. Daoud, *Appl. Surf. Sci.* 324 (2015) 532–537.

[3] K. Wang, F. Jia, Z. Zheng, L. Zhang, *Electrochem. Commun.* 12 (2010) 1764–1767.

[4] Y. Zhang, Q. Pei, J. Liang, T. Feng, X. Zhou, H. Mao, W. Zhang, Y. Hisaeda, X.M. Song, *Langmuir* 31 (2015) 10279–10284.

[5] S. Sfaelou, D. Raptis, V. Dracopoulos, P. Lianos, *RSC Adv.* 5 (2015) 95813–95816.

[6] K. Wang, F. Jia, L. Zhang, *Mater. Lett.* 92 (2013) 354–357.

[7] C.J. Brinker, G.C. Frye, A.J. Hurd, C.S. Ashley, *Thin Solid Films* 201 (1991) 97–108.

[8] L. Cisneros-Zevallos, J.M. Krochta, *J. Food Sci.* 68 (2003) 503–510.

[9] M. Mennig, P.. Oliveira, A. Frantzen, H. Schmidt, *Thin Solid Films* 351 (1999) 225–229.

[10] T. Bottein, J. Loizillon, D. Grosso, *J. Phys. Chem. B* 121 (2017) 6220–6225.

[11] S.J. Weinstein, K.J. Ruschak, *Chem. Eng. Sci.* 56 (2001) 4957–4969.

[12] A. Eberle, A. Reich, *J. Non. Cryst. Solids* 218 (1997) 156–162.

[13] J.A. Tallmadge, *AIChE J.* 17 (1971) 243–246.

[14] N.J. Arfsten, A. Eberle, J. Otto, A. Reich, *J. Sol-Gel Sci. Technol.* 8 (1997) 1099–1104.

[15] M. Fang, H. Jia, W. He, Y. Lei, L. Zhang, Z. Zheng, *Phys. Chem. Chem. Phys.* 17 (2015) 13531–13538.

[16] Y. Park, Y. Na, D. Pradhan, B.-K. Min, Y. Sohn, *CrystEngComm* 16 (2014) 3155–3167.

[17] X. Xiao, W.-D. Zhang, *J. Mater. Chem.* 20 (2010) 5866–5870.

[18] J. Cao, B. Xu, H. Lin, B. Luo, S. Chen, *Dalt. Trans.* 41 (2012) 11482.

[19] D.S. Bhachu, S.J.A. Moniz, S. Sathasivam, D.O. Scanlon, A. Walsh, S.M. Bawaked, M. Mokhtar, A.Y. Obaid, I.P. Parkin, J. Tang, C.J. Carmalt, *Chem. Sci.* 7 (2016) 4832–4841.

[20] J. Cao, B. Xu, H. Lin, B. Luo, S. Chen, *Dalt. Trans.* 41 (2012) 11482.

[21] M.A. Butler, *J. Appl. Phys.* 48 (1977) 1914–1920.

[22] K.-L. Zhang, C.-M. Liu, F.-Q. Huang, C. Zheng, W.-D. Wang, *Appl. Catal. B Environ.* 68 (2006) 125–129.

[23] R. Jiang, H. Zhu, X. Li, L. Xiao, *Chem. Eng. J.* 152 (2009) 537–542.

[24] J. Cao, B. Luo, H. Lin, S. Chen, *J. Mol. Catal. A Chem.* 344 (2011) 138–144.

[25] Y. Wang, K. Deng, L. Zhang, *J. Phys. Chem. C* 115 (2011) 14300–14308.

[26] X. Chang, J. Huang, Q. Tan, M. Wang, G. Ji, S. Deng, G. Yu, *Catal. Commun.* 10 (2009) 1957–1961.

[27] Y. Lei, G. Wang, S. Song, W. Fan, M. Pang, J. Tang, H. Zhang, *Dalt. Trans.* 39 (2010) 3273–3278.

[28] X. Xiao, W.-D. Zhang, *J. Mater. Chem.* 20 (2010) 5866–5870.

[29] H. Cheng, B. Huang, Y. Dai, X. Qin, X. Zhang, *Langmuir* 26 (2010) 6618–6624.

[30] W.W. Lee, C.-S. Lu, C.-W. Chuang, Y.-J. Chen, J.-Y. Fu, C.-W. Siao, C.-C. Chen, *RSC Adv.* 5 (2015) 23450–23463.

[31] Y.R. Jiang, H.P. Lin, W.H. Chung, Y.M. Dai, W.Y. Lin, C.C. Chen, *J. Hazard. Mater.* 283 (2015) 787–805.

[32] Y.-R. Jiang, S.-Y. Chou, J.-L. Chang, S.-T. Huang, H.-P. Lin, C.-C. Chen, *RSC Adv.* 5 (2015) 30851–30860.

[33] O. Özakın, B. Güzeldir, M.A. Yıldırım, M. Sağlam, A. Ateş, *Phys. Status Solidi* 209 (2012) 687–693.

[34] N.T. Hahn, S. Hoang, J.L. Self, C.B. Mullins, *ACS Nano* 6 (2012) 7712–7722.

# CHAPTER 3

# EFFECT OF PRECURSOR CONCENTRATION ON THE PROPERTIES OF BISMUTH OXYIODIDE FOR PHOTOVOLTAIC DEVICE

## 3.1. Introduction

Among the bismuth oxyhalide materials, BiOI is one of the attracted materials to be applied as semiconductor material [1]. It has been reported as a good material for photocatalyst [2–10] and it can be applied in the solar cell devices [10–16]. BiOI also has the band gap energy value ~1.8 eV with strong absorption in visible light region. However, the BiOI performance is still low, which is ~1% [12]. The condition during the semiconductor material preparation may be an important factor to increase the solar cell performance. In the BiOI synthesis, precursor condition (i.e. precursor and solvent adjustment [17–20], concentration [21–23], and surfactant selection [18,20]) can be the key factors to improve the materials properties, like morphology, size, crystallinity which those properties have an effect on the photovoltaic cell performance.

Generally, there are two types of BiOI synthesis ways, which need solvent and no need the solvent usage [10,15,24–27]. In the solvo-reaction method, BiOI films can be prepared by SILAR and chemical based deposition (CBD) [12,13,15]. In SILAR, the solar cell performance was influenced by the number of cycle reaction because it controls the thickness and other properties [12–15]. In addition, the angle inclination in SILAR has the effect on the BiOI solar cell performance [28]. Referring to the increment of CuO solar cell performance due to the increase in its precursor molarity in SILAR [29], the molarity precursor can be optimized to prepare BiOI films. The precursor concentration can control the morphology, structural and optical properties [30–32]. By adjusting the precursor concentration, there is a possibility to get

the desired film, reduce the amount of solvent and solute usage, and reduce the time needed for preparing the films [33].

Although the successful BiOI photoanode for solar cell application by SILAR with 5 mM of precursors was reported, its short-circuit current was not more than 1 mA/cm$^2$ [11–15]. Then, here, this chapter addresses the possibility of solar cell performance enhancement in BiOI films by varying its precursor concentration and report the double increment of Jsc value from the prepared BiOI films in this work compared with the previous results. Owing to the increase in the precursor concentration, the different properties of BiOI films and their solar cell performance were obtained. So far, there is no reported study in the precursor concentration effect during BiOI preparation using SILAR method.

## 3.2. Materials and method

The BiOI deposition onto the cleaned FTO substrate with the size 2 x 2 cm was done by modified SILAR [14] using varied $Bi(NO_3)_3.5H_2O$ and KI precursor concentrations (i.e 2 mM, 5 mM, 6 mM 7 mM, 8 mM, and 10 mM). In the deposition process, the lifting speed and the cycles were set up at 0.2 mm/s and 30 cycles respectively. All of the prepared films were heated in air at 100 $^oC$ for 1h.

The resulted films were utilized as photoanode. The Pt-coated glass was used as the counter electrode and $I^-/I_3^-$ redox (Solaronix Iodolyte AN-50) was for the electrolyte liquid media. The samples were test with a solar simulator (100 mW/cm$^2$, AM 1.5 illumination) in the air with the area 0.16 cm$^2$. Further characterization was tested by using X-Ray diffraction (XRD, Rigaku SmartLab), Raman Spectrometer (Raman, JASCO NRS-2100), UV-Visible NIR Spectroscopy (UV-Vis NIR Spectrophotometer, JASCO 670 UV), and Field Emission Scanning Electron Microscope (FESEM, JEOL JSM-7001F). The solar cell construction is shown in the Fig. 3.1.

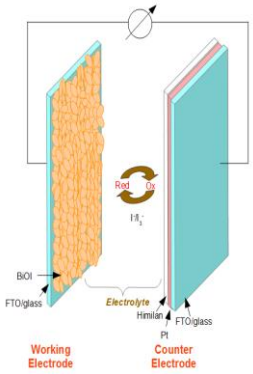


**Fig. 3.1** Illustration of BiOI solar cell.

## 3.3. Analysis of BiOI structure and morphology

### 3.3.1. Structural analysis

The diffractogram in Fig. 3.2 represents the XRD patterns of prepared BiOI films at 5 mM and 10 mM. The higher precursor concentration leads to the increase in the crystallinity of BiOI. It was easy to obtain the thicker BiOI film at the higher concentration which was supported by the higher intensity of BiOI peaks in the XRD patterns. The resulted BiOI crystal has good agreement with the previous report and JCPDS card no 73-2062 [26]. The character of BiOI was identified from the attributed peak at 2θ around $29.6^{o}$ (012), $31.7^{o}$ (110), and $45.5^{o}$ (020).

The crystal structure pattern of BiOI both in the films from 5 mM and 10 mM are qualitatively same. The only different thing comes from the full width at half maximum value (FWHM). It had the impact on the crystallite size of BiOI which was 16.94 and 18.46 nm from 5 and 10 mM of precursor concentration. Therefore, the higher molarity of precursors can result in the larger grain size of material. This is in line with the previous report [29].

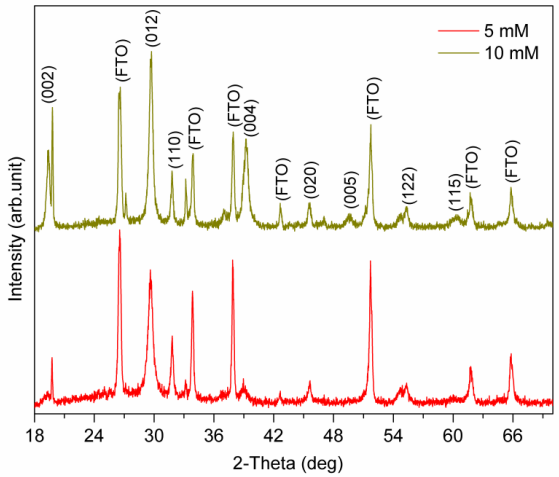


**Fig. 3.2** XRD patterns of BiOI films from 5 and 10 mM.

### 3.3.2. Morphological analysis

Fig. 3.3 shows the SEM images of BiOI films from 5 mM, 6 mM, 7 mM, and 10 mM of precursor concentration. The results are expressed in A, B, C, and D, respectively. The resulted films have the flake structure like in the previous research. By the same cycles, BiOI flakes cannot be clearly seen in the earlier concentration (5 mM), whilst, at the higher concentration, the wider flakes BiOI appeared. In Fig. 3.3B and 3.3C, the wider and thicker of BiOI flakes have the lateral size around 500 nm and more than 1 µm for BiOI in the Fig. 3.3D. The more and bigger rod-like material are obtained in the higher concentration. This phenomenon is similar to the previous report [34]. In Fig. 3.3E, the cross sectional image of BiOI film shows the BiOI thickness is ~3.4 µm-thick from the prepared BiOI at around 6 mM of precursor concentration.

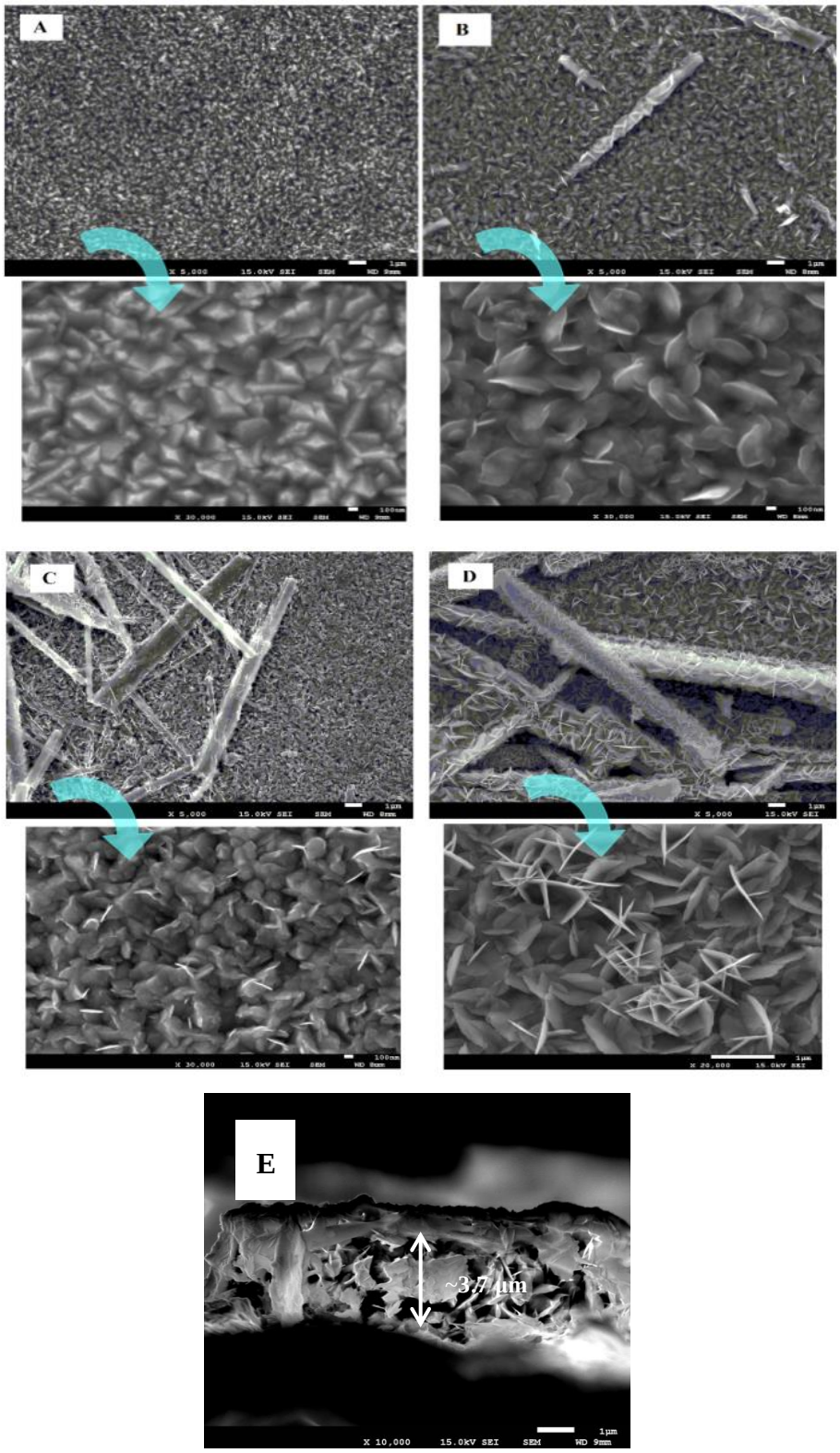


**Fig. 3.3** SEM image of BiOI films from the concentration: 5 mM (A), 6 mM (B), 7 mM (C), 10 mM (D) and cross sectional of ~6 mM of precursor (E).

The proposed illustration of BiOI growth is shown in Fig. 3.4. Within the concentration of 5 mM for 30 cycles, the wider BiOI flakes are obtained started from 6 mM. Rod-like materials which consisted of BiOI flakes can be obtained by the more concentrated precursors (7, 8, 10 mM). The reaction probability between anion and cation may be caused by the increase in the precursor concentration which enhances the probability collision among reactants in the concentrated solution. BiOI flakes also can result in the self-assembly formation of new morphology like flower-like structures of BiOI [4,35,36]. The rod-like material transformation from flakes morphology also could occur in the hematite synthesis [37].

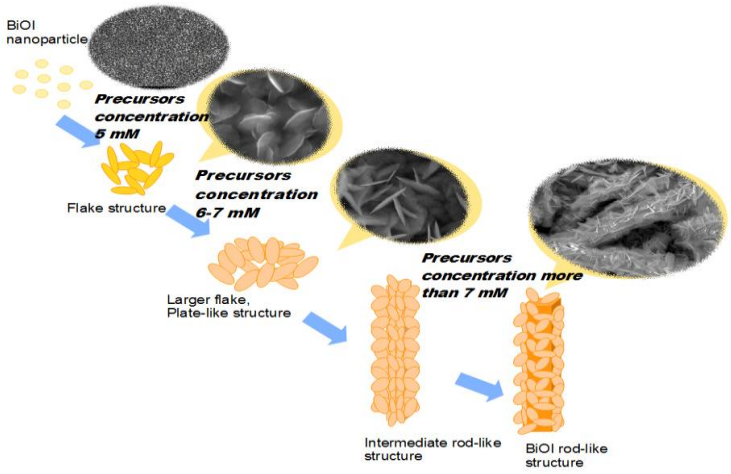


**Fig. 3.4** Proposed illustration of BiOI morphology changing due to the concentration effect.

## 3.4. Optical properties

### 3.4.1. UV-Visible spectral analysis

Fig. 3.5 shows the transmittance and absorbance spectra of BiOI films. The precursor concentration has the effect on the material absorption in the visible spectral range. The more concentrated of $Bi(NO_3)_3$ and KI resulted in the wider visible light range absorption and higher absorbance of BiOI films.

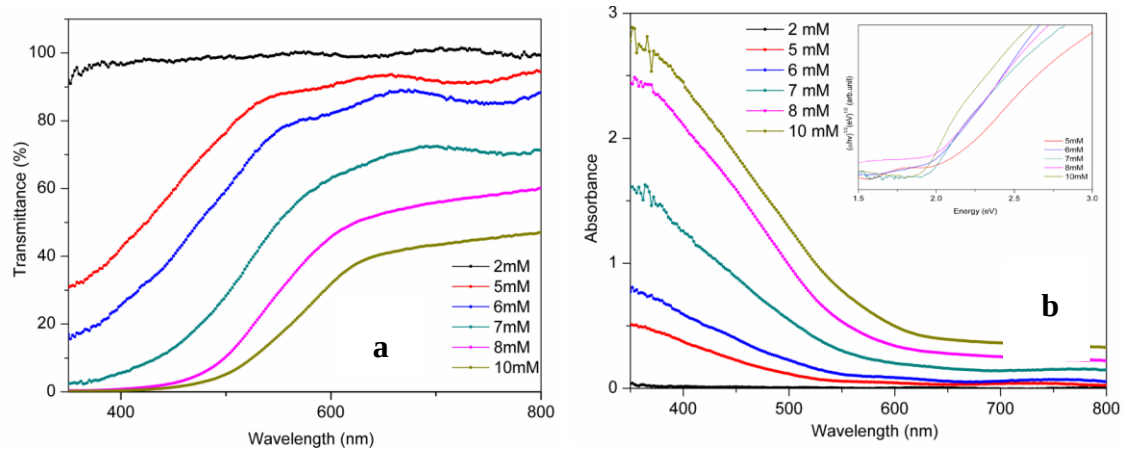


**Fig. 3.5** UV-Vis transmittance (a) and absorbance spectra of synthesized BiOI films in the precursor concentration (b). Inset: Tauc plot for indirect band gap calculation, $(\alpha hv)^{1/2}$ vs photon energy (hv).

The band gap energy calculation using Tauc plot for indirect band gap of BiOI is shown in Fig. 3.6. According to the $(\alpha hv)^{1/2}$ vs (hv) plot, the band gap energy of prepared BiOI films are varying from 1.85 eV to 1.7 eV. The result is also in good agreement with the absorbance data. The increase of BiOI grain size at the higher precursor molarity may change the BiOI band gap energy and it has the good agreement with the previous report [38].

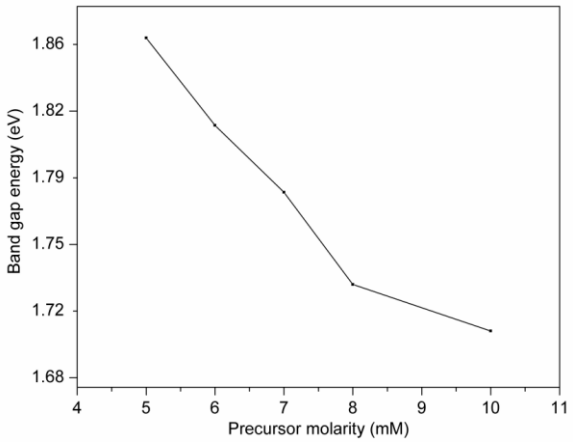


**Fig. 3.6** Band gap energy of resulted BiOI films prepared from the different concentration.

### 3.4.2. Raman analysis

Fig. 3.7 shows the Raman spectra of BiOI films. All of films have the strong peak which indicated Bi-I vibration stretching mode (Eg) at 147.91 $cm^{-1}$. It is in line with the previous results [39–43]. However, other peaks for BiOI Raman pattern could not be detected due to the limitation during the observation. This condition is similar to the previous report [39]. The increase in the Bi-I vibration peak may be affected by the amount of BiOI in the films. Hence, it is believed that the higher precursor molarity could induce the faster agglomeration and aggregation of BiOI particles to result in the more BiOI [44].

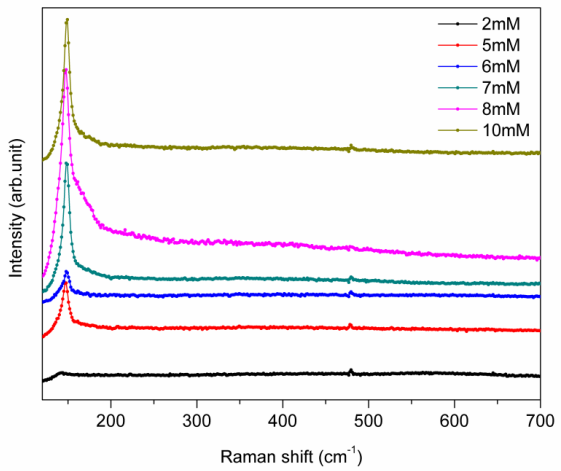


**Fig. 3.7** Raman spectra of BiOI films prepared from the different concentration.

## 3.5. Photovoltaic properties

The solar cell performance of BiOI films is displayed in the Fig. 3.8. From the I-V analysis, the improvement of solar cell performance is obviously seen up to the precursor concentration 7 mM. Then, it drops significantly when the concentration is increased up to 10 mM. This work shows the best efficiency of 0.318% for the BiOI photoanode prepared from 7 mM precursor solution. Although the solar cell performance is still low, it shows the photovoltaic performance

improvement of BiOI photoanode. The better performance of single BiOI photoanode for solar cell has been obtained in comparison to the previous results [13,14].

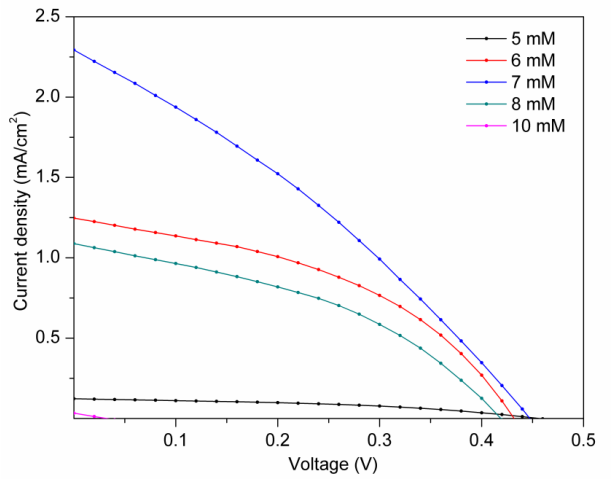


**Fig. 3.8** I-V performance of synthesized BiOI films prepared from the different concentration.

The effect of thickness and material size due to the changing precursor concentration may result in the higher visible light harvesting in BiOI films. However, sometimes it could decrease the solar cell parameter. The thicker layer may result in the non-compact layer which reduces the solar cell performance because of the increasing probability of back electron transfer in solar cell device. This phenomenon might be same as in the previous result [28] and it seems similar to the reported researches [10,12,14–16,45]. In this work, an extremely decreasing of photovoltaic performance is known to occur for resulted BiOI from 10 mM. Although the crystallinity between those prepared film by 5 mM and 10 mM had not a significant different, the Jsc and Voc of resulted materials at 10 mM of precursors was near from zero. The bigger size of BiOI and the thicker BiOI might influence the electron lifetime to make the solar performance of this film to be much lower.

The resulted EQE analysis is shown in the Fig. 3.9. In this work, the EQE peak and Jsc show the same trend although the efficiency of BiOI devices is still low in comparison to the Pb-

perovskite. The chemical composition and crystallographic structure of BiOI and Pb-perovskite are different but it has been predicted that those material are high-defect tolerant semiconductor materials [46] which may be beneficial for the solar cell device application.

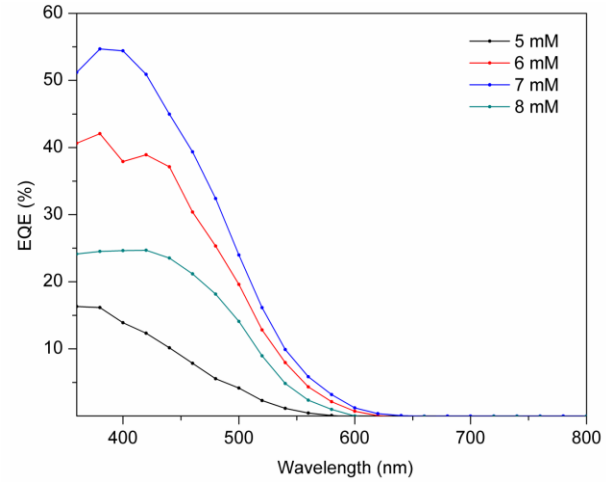


**Fig. 3.9** EQE curve of synthesized BiOI films from some precursor concentrations.

## 3.6. Conclusions

The precursor molarity variation in BiOI films preparation has the effect in the different physical properties of BiOI and further for solar cell application. Molarity of 7 mM was the best condition for BiOI preparation which resulted in the Jsc value of ~2.2 mA/cm$^2$. The thicker layer could be achieved easily in the higher concentration of $Bi(NO_3)_3$ and KI but it resulted in the bigger flaky and rod-like BiOI which decreased the solar cell performance. The increment of solar cell performance existed up to concentration 7 mM and drop significantly at 10 mM. Hence, it can be pointed that the physical properties of BiOI films prepared by SILAR can be strongly controlled by the molarity of precursor.

## 3.7. References

[1] A. Han, H. Zhang, G.K. Chuah, S. Jaenicke, *Appl. Catal. B Environ.* 219 (2017) 269–275.

[2] X. Chang, J. Huang, Q. Tan, M. Wang, G. Ji, S. Deng, G. Yu, *Catal. Commun.* 10 (2009)

1957–1961.

[3] H. Cheng, B. Huang, Y. Dai, X. Qin, X. Zhang, *Langmuir* 26 (2010) 6618–6624.

[4] Y. Wang, K. Deng, L. Zhang, *J. Phys. Chem. C* 115 (2011) 14300–14308.

[5] J. Cao, B. Xu, B. Luo, H. Lin, S. Chen, *Catal. Commun.* 13 (2011) 63–68.

[6] G. Dai, J. Yu, G. Liu, *J. Phys. Chem. C* 115 (2011) 7339–7346.

[7] G. Wang, J. Wang, P. Yang, *J. Nanosci. Nanotechnol.* 18 (2018) 309–313.

[8] X. Su, J. Yang, X. Yu, Y. Zhu, Y. Zhang, *Appl. Surf. Sci.* 433 (2018) 502–512.

[9] J. Niu, P. Dai, Q. Zhang, B. Yao, X. Yu, *Appl. Surf. Sci.* 430 (2018) 165–175.

[10] R.L.Z. Hoye, L.C. Lee, R.C. Kurchin, T.N. Huq, K.H.L. Zhang, M. Sponseller, L. Nienhaus, R.E. Brandt, J. Jean, J.A. Polizzotti, A. Kursumović, M.G. Bawendi, V. Bulović, V. Stevanović, T. Buonassisi, J.L. MacManus-Driscoll, *Adv. Mater.* 29 (2017) 1–10.

[11] L. Wang, W.A. Daoud, *Appl. Surf. Sci.* 324 (2015) 532–537.

[12] S. Sfaelou, D. Raptis, V. Dracopoulos, P. Lianos, *RSC Adv.* 5 (2015) 95813–95816.

[13] Y. Zhang, Q. Pei, J. Liang, T. Feng, X. Zhou, H. Mao, W. Zhang, Y. Hisaeda, X.M. Song, *Langmuir* 31 (2015) 10279–10284.

[14] K. Wang, F. Jia, L. Zhang, *Mater. Lett.* 92 (2013) 354–357.

[15] K. Wang, F. Jia, Z. Zheng, L. Zhang, *Electrochem. Commun.* 12 (2010) 1764–1767.

[16] Y. Zhang, Y. Li, W. Sun, C. Yuan, B. Wang, W. Zhang, X.M. Song, *Langmuir* 33 (2017) 12065–12071.

[17] J.-H. Huang, H.J. Parab, R.-S. Liu, T.-C. Lai, M. Hsiao, C.-H. Chen, H.-S. Sheu, J.-M. Chen, D.-P. Tsai, Y.-K. Hwu, *J. Phys. Chem. C* 112 (2008) 15684–15690.

[18] R. Hufschmid, H. Arami, R.M. Ferguson, M. Gonzales, E. Teeman, L.N. Brush, N.D. Browning, K.M. Krishnan, *Nanoscale* 7 (2015) 11142–11154.

[19] H. Zeng, P.M. Rice, S.X. Wang, S. Sun, *J. Am. Chem. Soc.* 126 (2004) 11458–11459.

[20] W. Baaziz, B.P. Pichon, S. Fleutot, Y. Liu, C. Lefevre, J.-M. Greneche, M. Toumi, T. Mhiri, S. Begin-Colin, *J. Phys. Chem. C* 118 (2014) 3795–3810.

[21] C.J. Meledandri, J.K. Stolarczyk, S. Ghosh, D.F. Brougham, *Langmuir* 24 (2008) 14159–14165.

[22] A. Demortière, P. Panissod, B.P. Pichon, G. Pourroy, D. Guillon, B. Donnio, S. Bégin-Colin, *Nanoscale* 3 (2011) 225–232.

[23] F.B. Effenberger, R.A. Couto, P.K. Kiyohara, G. Machado, S.H. Masunaga, R.F. Jardim, L.M. Rossi, *Nanotechnology* 28 (2017) 115603.

[24] X. Zhang, L. Zhang, T. Xie, D. Wang, *J. Phys. Chem. C* 113 (2009) 7371–7378.

[25] Y. Lei, G. Wang, S. Song, W. Fan, M. Pang, J. Tang, H. Zhang, *Dalt. Trans.* 39 (2010) 3273–3278.

[26] X. Xiao, W.-D. Zhang, *J. Mater. Chem.* 20 (2010) 5866–5870.

[27] Y. Long, Q. Han, Z. Yang, Y. Ai, S. Sun, Y. Wang, Q. Liang, M. Ding, *J. Mater. Chem. A* 6 (2018) 13005–13011.

[28] A.A. Putri, S. Kato, N. Kishi, T. Soga, *Jpn. J. Appl. Phys.* 58 (2019) SAAD09.

[29] S. Visalakshi, R. Kannan, S. Valanarasu, H.S. Kim, A. Kathalingam, R. Chandramohan, *Appl. Phys. A Mater. Sci. Process.* 120 (2015) 1105–1111.

[30] M. Soylu, M. Coskun, *J. Alloys Compd.* 741 (2018) 957–968.

[31] R. Irani, S.M. Rozati, S. Beke, *Appl. Phys. A Mater. Sci. Process.* 124 (2018) 321.

[32] U. Chaitra, D. Kekuda, K.M. Rao, *J. Mater. Sci. Mater. Electron.* 27 (2016) 7614–7621.

[33] N.J. Arfsten, A. Eberle, J. Otto, A. Reich, *J. Sol-Gel Sci. Technol.* 8 (1997) 1099–1104.

[34] N. Moloto, N. Revaprasadu, P.L. Musetha, M.J. Moloto, *J. Nanosci. Nanotechnol.* 9 (2009) 4760–4766.

[35] Y. Liu, J. Xu, L. Wang, H. Zhang, P. Xu, X. Duan, H. Sun, S. Wang, *Nanomaterials* 7 (2017) 64.

[36] J. Hou, K. Jiang, M. Shen, R. Wei, X. Wu, F. Idrees, C. Cao, *Sci. Rep.* 7 (2017) 11665.

[37] T. Liu, Y. Ling, Y. Yang, L. Finn, E. Collazo, T. Zhai, Y. Tong, Y. Li, *Nano Energy* 12 (2015) 169–177.

[38] J. Raj Mohamed, L. Amalraj, *J. Asian Ceram. Soc.* 4 (2016) 357–366.

[39] Y. Park, Y. Na, D. Pradhan, B.-K. Min, Y. Sohn, *CrystEngComm* 16 (2014) 3155–3167.

[40] J. Cao, B. Xu, H. Lin, B. Luo, S. Chen, *Dalt. Trans.* 41 (2012) 11482.

[41] M. Long, P. Hu, H. Wu, Y. Chen, B. Tan, W. Cai, *J. Mater. Chem. A* 3 (2015) 5592–5598.

[42] W. Fan, H. Li, F. Zhao, X. Xiao, Y. Huang, H. Ji, Y. Tong, *Chem. Commun.* 52 (2016) 5316–5319.

[43] M. Fang, H. Jia, W. He, Y. Lei, L. Zhang, Z. Zheng, *Phys. Chem. Chem. Phys.* 17 (2015) 13531–13538.

[44] P.N. Sibiya, M.J. Moloto, *Chalcogenide Lett.* 11 (2014) 577–588.

[45] X. Zhang, L. Zhang, *J. Phys. Chem. C* 114 (2010) 18198–18206.

[46] L.C. Lee, T.N. Huq, J.L. Macmanus-Driscoll, R.L.Z. Hoye, *APL Mater.* 6 (2018) 084502.

# CHAPTER 4

# PREPARED BISMUTH OXYIODIDE BY SPIN-SILAR FOR PHOTOVOLTAIC APPLICATION

## 4.1. Introduction

BiOI is one of semiconductor materials which is considered to have the high-defect tolerance property although bismuth is listed in a heavy metal member [1]. BiOI can be clustered as p-type semiconductor with the narrow band gap and strong absorption under visible light at ~1.8 eV of band gap energy value. Therefore, owing to its character which is safe to environment, BiOI has been commonly applied in photocatalytic reaction and photovoltaic device [2,3]. Typically, BiOI can be synthesized by dip-SILAR [2], chemical vapor transport [4], mechanical grinding [5], and solvo-thermal reaction [6].

In the conventional dip-SILAR, the rinsing step must be involved to maintain the film uniformity in order to get the better performance. However, due to the water treatment, this dip-SILAR consumes the more time for producing the better film, particularly in the large-scale BiOI fabrication. Then, it is considered that dip-SILAR has less reproducibility despite the fact that it is low cost [7]. Furthermore, the surface morphology becomes worse with the film thickening due to the remaining solution after a repeated dip-coating up to 30 cycles [8]. Since adsorption and reaction can occur while the spin-coating process is running, this chapter proposes spin-SILAR to deposit BiOI onto the substrates to prepare a flat film in short time for the first time. By utilizing this method, the rinsing step and drying process can be completed when the solution are spun [9]. In addition, only the small amount of precursor solution is required in spin-coating

and thanks to the less remaining waste solution in spin-SILAR, for this reason, it offers the opportunity to be more environmentally benign than dip-SILAR.

In this chapter, the structural, optical, and photovoltaic properties of BiOI film deposition by spin-SILAR instead of the conventional dip-SILAR are studied. The deposited BiOI films onto FTO/glass substrates exhibited the better performance of solar cell device with Pt/FTO as counter electrode and $I^-/I_3^-$ solution as electrolyte compared to the previous result [2]. BiOI films preparation by spin-SILAR with changing the number of cycle was adapted from the previous experiment [2]. By the morphological analysis, the better uniformity of resulted BiOI layer by spin-SILAR was obtained although the rinsing step was eliminated. To date, there is no reported BiOI film deposition and its application involving spin-SILAR for photovoltaic devices.

## 4.2. Synthesis and fabrication of BiOI films

20 mg $Bi(NO_3)_3.5H_2O$ as bismuth source was dissolved in 5 mL deionized water. The same mole ratio of KI as iodide solution was also prepared. For the cleaning step of glass substrate, a sequential washing for 3 times in organic solvents, like acetone (twice) and ethanol (once) for 5 minutes each was followed with $N_2$ gas blowing and $UV/O_3$ treatment for 30 minutes in total. To deposit BiOI films, bismuth and potassium precursors were dropped separately onto the cleaned FTO glass substrates before spin-coating process. Spin-coating was carried out for 20 s at 1500 rpm. One cycle reaction completed if a sequential dropwise of bismuth solution was followed by potassium solution dropping onto the substrates. The preparation of BiOI films by SILAR using spin-coating method is illustrated in the Fig. 4.1 and the number of cycles in this experiment was set up from 5 up to 30 cycles. The thickness of the film was estimated using cross sectional image FESEM.

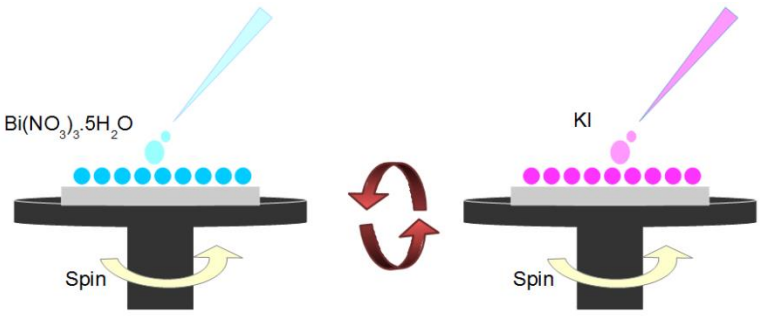


**Fig. 4.1** Schematic diagram of spin-SILAR process.

All of the resulted films were then characterized using X-Ray Diffraction (Rigaku RINT-2100 diffractometer), Raman Spectrometer (JASCO NRS-2100), FESEM JEOL JSM-7800F, and UV-Visible Spectroscopy (JASCO 670 UV). Solar cell structure was prepared by a sandwich structure using FTO glass substrate, adapted from dye-sensitized solar cell device without involving the dye solution [2]. The photovoltaic structure was arranged by FTO/BiOI photoanode and Platinum-based as a counter electrode, like the arrangement: FTO/BiOI films/Iodine electrolyte/Pt-FTO. Then, this structure was tested using solar simulator (100 $mW/cm^2$; AM 1.5 illumination) with 0.16 $cm^2$ illumination area.

## 4.3. Structural analysis

### 4.3.1. X-ray powder diffraction analysis

The diffraction patterns of BiOI films using spin-SILAR for various cycles are shown in the Fig. 4.2. The peaks in the diffractogram are in line with the crystal types in the JCPDS card 01-073-2062. It is obviously seen that the film crystallinity enhances due to the more reaction cycle. However, in the films, only two types of BiOI crystal planes are obtained via spin-SILAR, namely (001) and (102) plane which exist in 2θ at 9.76° and 29.6°. All of crystal patterns are dominated by the (001) crystal plane. Therefore, it can be assumed that the formation of BiOI crystal in this chapter was initiated by (001) plane growth. In the resulted BiOI films by dip-

coating, it is noticed that (102) and (110) planes were existed by the conventional SILAR and it was found that its crystallite size was around 18-21 nm. By involving the Debye-Scherrer equation in Eq. 2.2 [10], it can be obtained the crystallite size of BiOI from 15 and 30 cycles of spin-SILAR which were around 13.95 and 14.78 nm. The smaller crystal size may be obtained from the spin-coated BiOI sample in the less cycle, like in the BiOI film from 10 cycles.

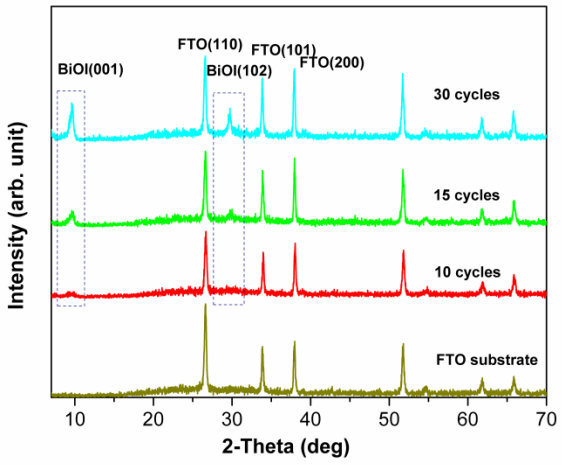


**Fig. 4.2** XRD patterns of prepared BiOI films by spin-SILAR.

### 4.3.2. Raman analysis

Fig. 4.3 shows the BiOI character in Raman spectra. All available peaks in this figure correspond to the Eg stretching mode of Bi-I vibration in BiOI. Although the impurity is not found in Raman spectra, it is observed that the crystal plane in BiOI may have an impact on the Raman peak shifting. Generally, BiOI with (110) crystal peak has the Eg peak around 147-149 $cm^{-1}$ [11,12]. However, the prepared BiOI via spin-coating process shifts to the Eg position 150.06 $cm^{-1}$ after 15 cycles. This peak position for BiOI character was also reported for BiOI Raman spectra with the stronger peak crystal plane in (001) [13]. In addition, the BiOI formation follows the chemical reaction in the Eq. 4.1 [14].

$$Bi^{3+} + I^{-} + H_2O \rightarrow BiOI + 2H^{+} \quad (4.1)$$

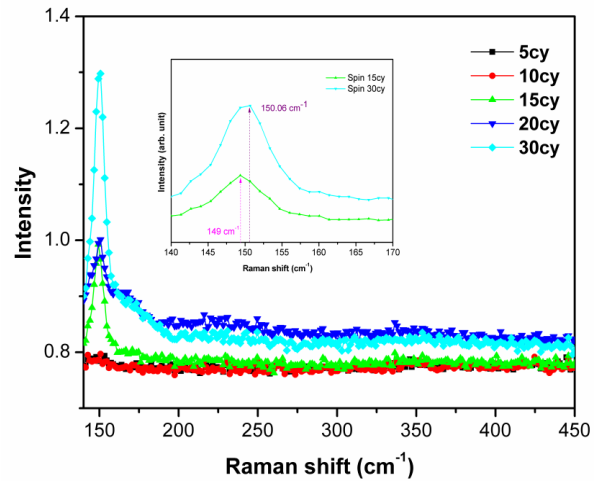


**Fig. 4.3** Raman spectra of prepared BiOI films by spin-SILAR.

### 4.3.3. Morphology analysis

By the FESEM analysis, it can be observed that the 30 cycles of BiOI film had the dense and compact film in comparison to the dip-SILAR result [8,15]. A more uniform of flake-like structure was obtained in this experiment as shown in the Fig. 4.4. It can be identified the flaky structure in the samples which is known as the basic shape of BiOI and it is also similar to the many reported researches. When the cycle reaction increases during the film preparation, it can result in the higher size and density of deposited BiOI which are shown by the lateral size of BiOI flake growth (see Fig 4.4a-c). After 30 reaction cycles, the BiOI films could display the clear flaky morphology (Fig. 4.4c), whereas its lateral size was half of the resulted BiOI by dip-coating, around 300 nm with the flake thickness around 10 nm [8]. The dip-coating process without rinsing step might initiate the further reaction between the remained $BiO^+$ in the substrate and iodide ion which induced in the bigger BiOI growth like shown in the previous report [8,15].

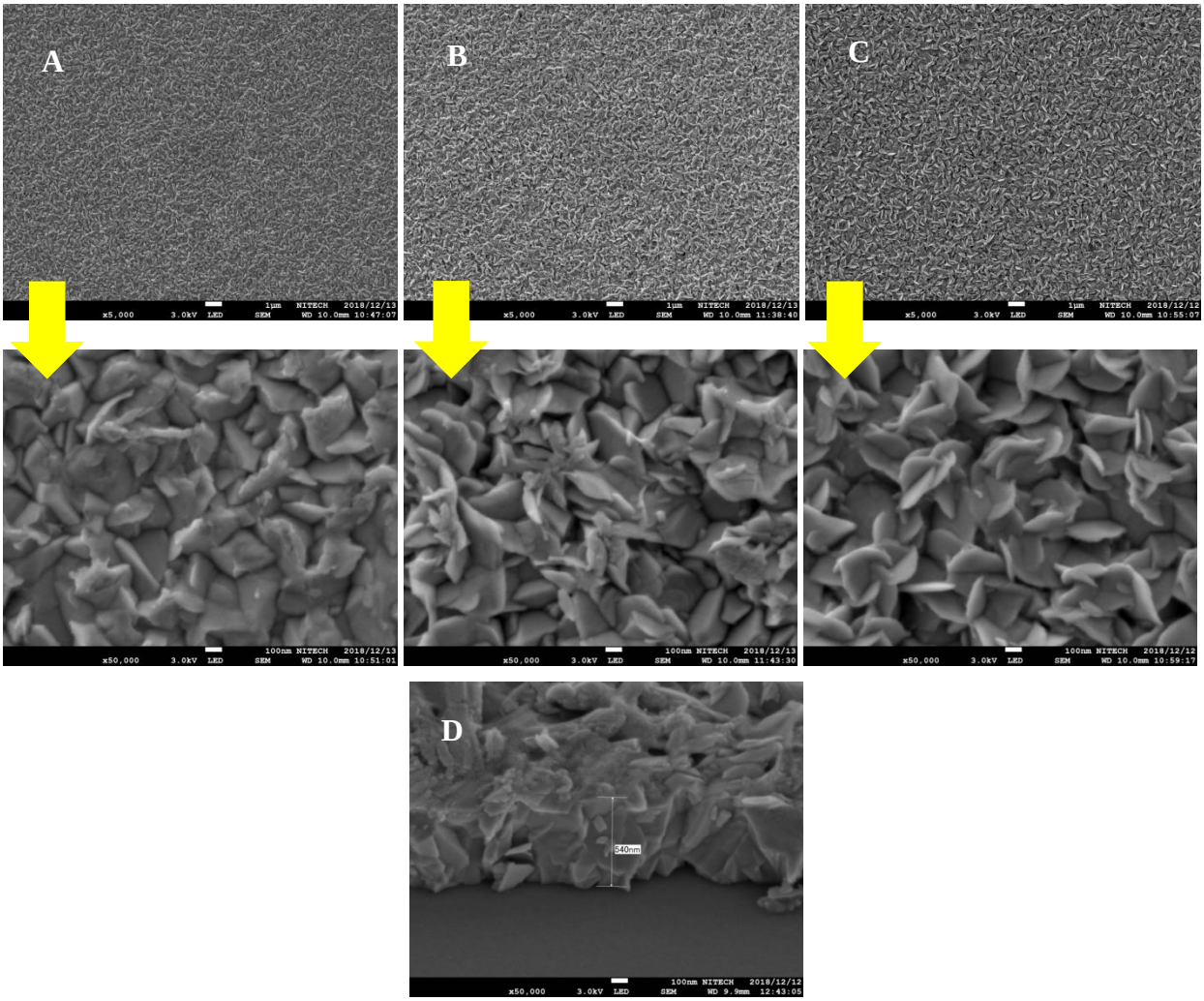


**Fig. 4.4** Top-view FESEM images of BiOI film from 10 cycles (a); 15 cycles (b); 30 cycles (c); and tilted image of BiOI film via spin-SILAR 30 cycles (d).

The compact BiOI film by spin-coating is shown in Fig. 4.4d, which tend to be denser than the previous dip-coated BiOI result [8,15]. Hence, owing to its smaller size, the prepared BiOI from spin-coating may have the higher surface area which can be expected to give a better performance. The interesting point of this process is the uniform films are easily produced via spin-SILAR.

## 4.4. Optical properties

The optical study in Fig. 4.5a shows the absorption spectra, A (λ) for BiOI/FTO in UV–Vis-NIR regions. The wider visible absorption of BiOI films due to the different cycle also can be reflected by the transmittance (see Fig. 4.5b) and reflectance spectra (see Fig. 4.5c). The greater film thickness and size of BiOI materials have the impact which is not only on the decrease in transmittance spectra, but also for the longer shifting in its absorption edge like shown in the Fig. 5.5 (a, b) and reported research [16]. Owing to the grain size increment, the film thickness will improve the maximum wavelength shifting [17]. The variation of the absorption coefficient with the photon energy is also given by Tauc's relation [18]:

$$\alpha h\nu = B(h\nu - E_g^{Opt})^r \qquad (4.2)$$

The best fitting of the experimental data to Eq. 4.2 is obtained when r = 2, so that, the type of electronic transition is indirect allowed transition, which is illustrated in Fig. 4.6. The calculated $E_g^{Opt}$ is in the range of BiOI band gap energy [19]. It is noticed that the band gap estimation shows the changing in the band gap energy value among the resulted BiOI films. However, since the resulted film by 5 cycles of spin-SILAR was very thin, it was difficult to calculate its band gap energy. Generally, the increase in the reaction cycles results in the $E_g^{Opt}$ decrease in BiOI films which may reflect on the film thickness. Therefore, the evaluation of band gap energy of BiOI films can be arranged for the following order: 30 cycles (1.95eV) < 20 cycles (1.95eV) < 15 cycles (2eV) < 10 cycles (2.25eV).

In addition, Raman's peak intensity of BiOI films in Fig. 4.3 shows an improvement due to the increasing of SILAR's cycle reaction number. The highest intensity of BiOI films is shown by the film from 30 reaction cycles via spin-SILAR. This character might be reflected by its film thickness which tuned the different value of band gap energy among the prepared BiOI films.

Furthermore, the band gap energy changing can be caused by the different lattice strains, dislocation of film densities, and crystallite size of semiconductor materials.

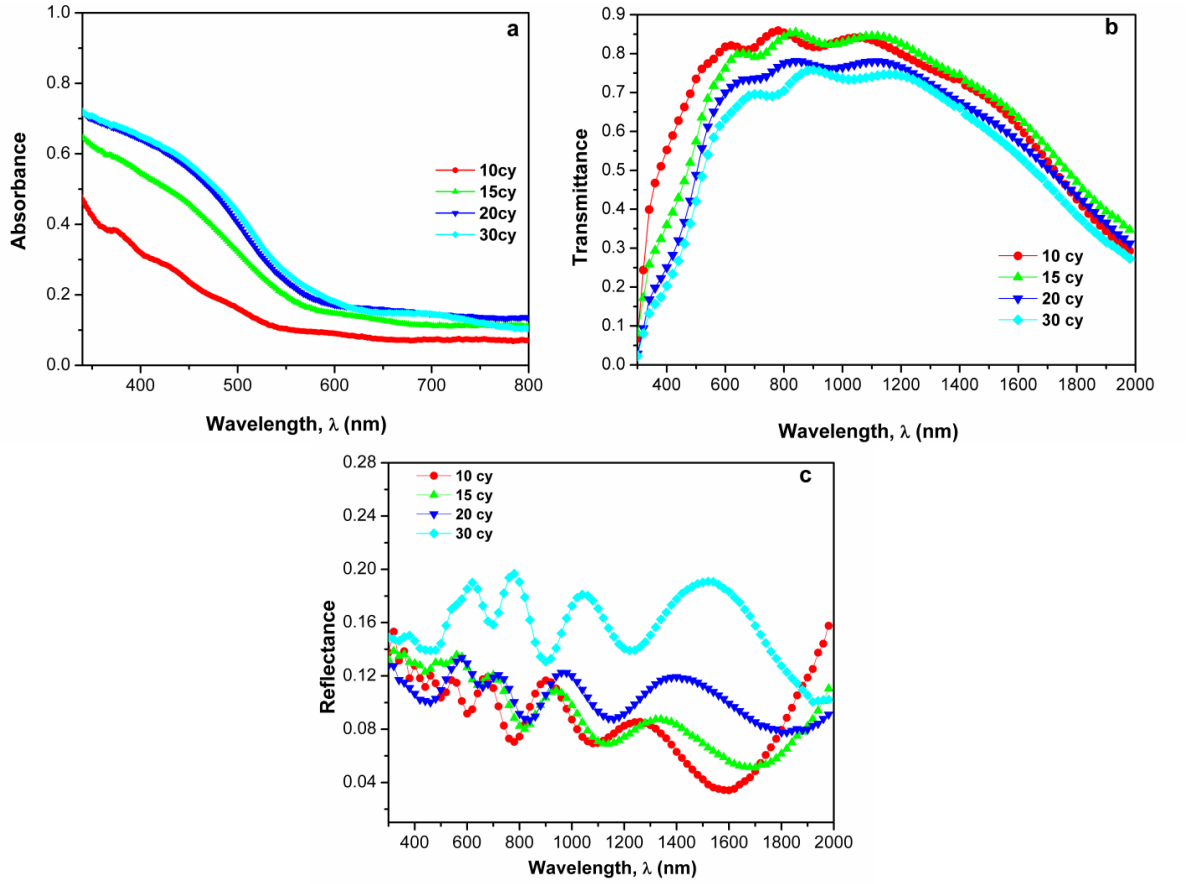


**Fig. 4.5** UV-Visible absorbance (a), transmittance (b) and reflectance spectra (c) of prepared BiOI films by spin-SILAR.

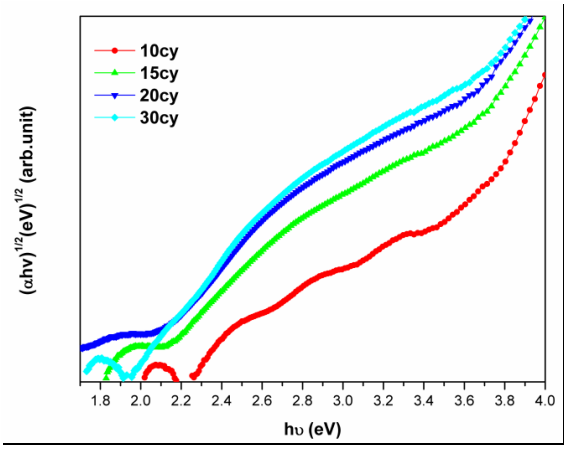


**Fig. 4.6** The band-gap energy calculation of prepared BiOI films by spin-SILAR.

## 4.5. Photovoltaic cell measurement

BiOI films exhibit the low efficiency of solar cell which is around 600 μA/cm$^2$ of Jsc. The solar cell evaluation by involving the iodine electrolyte as in the structure: FTO/BiOI/Iodine/Pt-FTO shows the data like it is displayed in the Fig. 4.7. The more BiOI film in the solar cell exhibits the higher solar cell parameter although after 15 cycles, it performs the decrease in its performance as it is shown in the Fig. 4.8. The same trend has been similar to the previous work [20]. In this work, the best short-circuit current and open-circuit voltage was exhibited by BiOI films from 15 cycles. By increasing the cycles, it had the impact on the increasing in its open-circuit voltage.

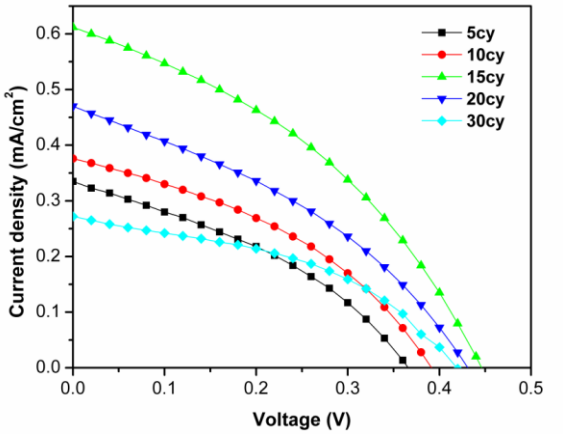


**Fig. 4.7** I -V curve prepared BiOI films by spin-SILAR in the different reaction cycle.

In addition, the centrifugal force in the spin-coating might play the important role to accelerate the solvent evaporation. As a consequence, the dense of BiOI films in the FTO substrates can be completed by spin-SILAR. The more (001) plane in the BiOI may be unpleasant for solar cell application since the solar cell performance declines due to the film thickening and (001) intensity increment. Since the distinct in the crystal type has the influence in the charge photogeneration, it had the impact on the solar cell performance and the photocatalytic activity of BiOI [14] compared to the previous results [8,15]. However, it is still

possible to tailor the facet orientation in BiOI films via spin-SILAR which is favorable for solar cell application and showing the better photovoltaic performance and apply this result for the solid solar cell based on the BiOI films.

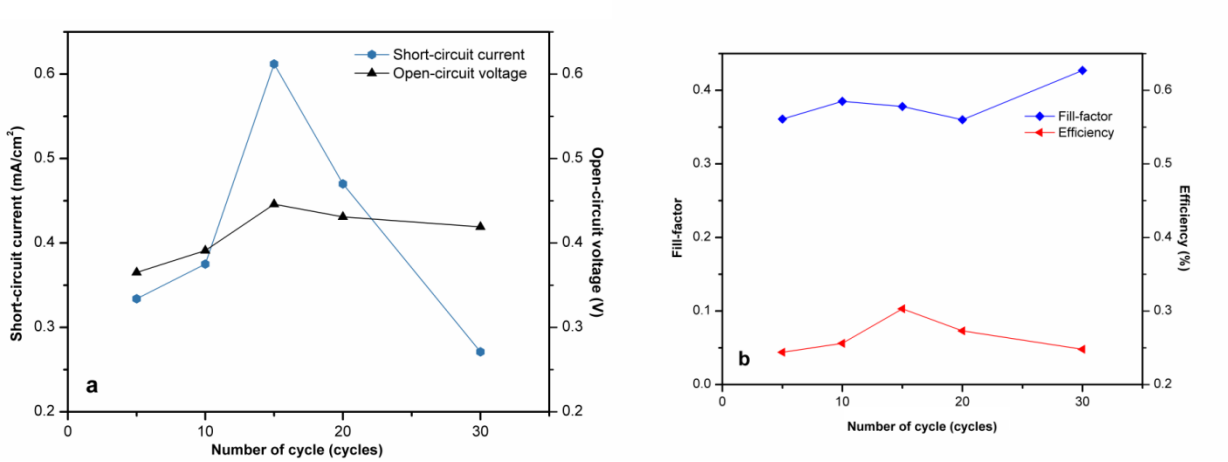


**Fig. 4.8** Short-circuit current and open-circuit voltage (a); and fill factor and efficiency (b) plots of prepared FTO/BiOI films by spin coating with cycle reaction variation.

## 4.6. Conclusions

In this chapter, spin-SILAR was proposed for the growth of BiOI films for the first time and by the solar cell analysis, it achieved the best solar cell parameter of 612 μA/cm$^2$; 0.446 V; and 0.103 % for its Jsc, Voc, and PCE, respectively. A good quality of BiOI film can be obtained by spin-coating process although the washing step was eliminated. Due to the time efficiency, simplicity and reproducibility of spin-SILAR, it is considered that this method can be aimed to the wider BiOI application. The crystal quality and quantity in the resulted films can be modified by the different precursor condition during this process.

## 4.7. References

[1] L.C. Lee, T.N. Huq, J.L. Macmanus-Driscoll, R.L.Z. Hoye, *APL Mater.* 6 (2018) 084502.

[2] K. Wang, F. Jia, L. Zhang, *Mater. Lett.* 92 (2013) 354–357.

[3] J. Lu, J. Wu, W. Xu, H. Cheng, X. Qi, Q. Li, Y. Zhang, Y. Guan, Y. Ling, Z. Zhang,

*Mater. Lett.* 219 (2018) 260–264.

[4] R.L.Z. Hoye, L.C. Lee, R.C. Kurchin, T.N. Huq, K.H.L. Zhang, M. Sponseller, L. Nienhaus, R.E. Brandt, J. Jean, J.A. Polizzotti, A. Kursumović, M.G. Bawendi, V. Bulović, V. Stevanović, T. Buonassisi, J.L. MacManus-Driscoll, *Adv. Mater.* 29 (2017) 1–10.

[5] Y. Long, Q. Han, Z. Yang, Y. Ai, S. Sun, Y. Wang, Q. Liang, M. Ding, *J. Mater. Chem. A* 6 (2018) 13005–13011.

[6] Y. Lei, G. Wang, S. Song, W. Fan, M. Pang, J. Tang, H. Zhang, *Dalt. Trans.* 39 (2010) 3273–3278.

[7] J. Joo, D. Kim, D.J. Yun, H. Jun, S.W. Rhee, J. Sung Lee, K. Yong, S. Kim, S. Jeon, *Nanotechnology* 21 (2010).

[8] A.A. Putri, S. Kato, N. Kishi, T. Soga, *Jpn. J. Appl. Phys.* 58 (2019) SAAD09.

[9] J.H. Heo, M.H. Jang, M.H. Lee, M.S. You, S.-W. Kim, J.-J. Lee, S.H. Im, *RSC Adv.* 7 (2017) 3072–3077.

[10] A.A. Abuelwafa, A. El-Denglawey, M. Dongol, M.M. El-Nahass, T. Soga, *Opt. Mater. (Amst).* 49 (2015) 271–278.

[11] Y. Park, Y. Na, D. Pradhan, B.-K. Min, Y. Sohn, *CrystEngComm* 16 (2014) 3155–3167.

[12] M. Fang, H. Jia, W. He, Y. Lei, L. Zhang, Z. Zheng, *Phys. Chem. Chem. Phys.* 17 (2015) 13531–13538.

[13] H. Li, Z. Yang, J. Zhang, Y. Huang, H. Ji, Y. Tong, *Appl. Surf. Sci.* 423 (2017) 1188–1197.

[14] R. He, J. Zhang, J. Yu, S. Cao, *J. Colloid Interface Sci.* 478 (2016) 201–208.

[15] A.A. Putri, S. Kato, N. Kishi, T. Soga, *J. Sci. Adv. Mater. Devices* 4 (2019) 116–124.

[16] J.S. Zhu, X.M. Lu, W. Jiang, W. Tian, M. Zhu, M.S. Zhang, X.B. Chen, X. Liu, Y.N. Wang, *J. Appl. Phys.* 81 (1997) 1392.

[17] F. Tepehan, N. Özer, *Sol. Energy Mater. Sol. Cells* 30 (1993) 353–365.

[18] S.M. Salem, E.K. Abdel-Khalek, E.A. Mohamed, M. Farouk, *J. Alloys Compd.* 513 (2012) 35–43.

[19] A.M. Ganose, M. Cuff, K.T. Butler, A. Walsh, D.O. Scanlon, *Chem. Mater.* 28 (2016) 1980–1984.

[20] S. Sfaelou, D. Raptis, V. Dracopoulos, P. Lianos, *RSC Adv.* 5 (2015) 95813–95816.

# CHAPTER 5

# BISMUTH OXYIODIDE AND ITS DERIVATION FROM ANNEALING TREATMENT FOR PHOTOVOLTAIC APPLICATION

## 5.1. Introduction

BiOI is a p-type semiconductor which can be applied for photocatalyst in photocatalytic reaction during the last decade [1–9]. This is also can be considered as the safe semiconductor material [10]. Besides for photocatalytic reaction, it is also useful for photoelectrochemical devices [11–17]. It can be synthesized both in the solvent usage and solventless condition [5,11,16,18–20]. Hydrothermal and solvo-thermal methods are commonly used for BiOI preparation in photocatalytic purposes [9,18,19]. Successive ionic layer adsorption and reaction (SILAR), and chemical-based deposition (CBD) are common to deposit BiOI films for photovoltaic application [13,14,16]. Here, the BiOI films preparation for solar cell was conducted via doctor blade method.

The morphology, size, crystallinity, and optical properties can be modified by the treatment during the materials preparation, the different concentration of precursors [21–23], and the different surfactant and solvent used [24,25]. In addition, the post-treatment like heating and calcination process can change the material properties. In BiOI, the calcination allows to produce BiOI derivation [26]. Also, the pH adjustment during the synthesis process can result in the different property of BiOI [1].

BiOI and the family member have been applied as the photocatalytic materials [27]. Like $Bi_4O_5I_2$, it could show the better photocatalytic performance than BiOI [28]. $Bi_7O_9I_3$ had the excellent photocatalytic activity under visible light irradiation [26,29]. $Bi_5O_7I$ could exhibit the twice higher of photocatalytic activity than BiOI [30]. Last, the polymorph $Bi_2O_3$ could show the

different order photocatalytic activity: $\beta - Bi_2O_3 > \alpha - Bi_2O_3 > \delta - Bi_2O_3$ [31]. However, up to date, there is no study in the screening of BiOI and its derivations for photovoltaic device application even though BiOI and its family have been considered as the promising material [11]. Therefore, this chapter discusses about the effect of annealing treatment of BiOI in the various temperature on the properties' material and their performance in photovoltaic device. The different temperature treatment resulted in the different performance of solar cell device.

## 5.2. Synthesis and fabrication of BiOI films

2 mmol $Bi(NO_3)_3.5H_2O$ and KI as solid precursors were grinded for 15 minutes. It was followed by adding 40 mL of deionized water which resulted in the orange mixture as-BiOI. Then, the as-BiOI was stirred for 5 h at room temperature to obtain BiOI powder. Rinsing treatment was carried out for BiOI powder with ethanol and deionized water for several times. To prepare the BiOI films via doctor blade method, the BiOI paste was made by mixing BiOI with ethanol for 5 minutes in the homogenizer. Eventually, the deposited BiOI on FTO substrates were heated at a different temperature, i.e 100 $^oC$; 200 $^oC$; 300 $^oC$; 450 $^oC$; and 550 $^oC$ for 1 h. The film thickness was around 1.5 μm.

All of the resulted films were utilized as photoanode. The Pt-coated glass was used as the counter electrode and $I^-/I_3^-$ redox (Solaronix Iodolyte AN-50) was for the electrolyte liquid media. The samples were test with a solar simulator (100 mW/cm$^2$, AM 1.5 illumination) in the air with the area 0.16 cm$^2$. Further characterization was carried out by using X-Ray diffraction (XRD, Rigaku SmartLab), Raman Spectrometer (Raman, JASCO NRS-2100), UV-Visible NIR Spectroscopy (UV-Vis NIR Spectrophotometer, JASCO 670 UV), and Field Emission Scanning Electron Microscope (FESEM, JEOL JSM-7001F).

## 5.3. Structural and morphological analysis

### 5.3.1. XRD analysis

XRD patterns of BiOI and its family are showed in Figure 5.1. The different XRD patterns are obviously seen in Fig. 5.1. The treatment at 100 $^{o}$C displays the BiOI character which is in line to the JCPDS card of BiOI no. 00-73-2062. The crystal planes (001); (002); (102); (110); (013); (004); (200); (114); and (122) are located at 2θ around 9.6$^{o}$; 19.3$^{o}$; 29.8$^{o}$; 31.86$^{o}$; 36.8$^{o}$; 39.2$^{o}$; 45.8$^{o}$; 51.2$^{o}$; and 55$^{o}$. The similar pattern of annealed BiOI at 200 and 300 $^{o}$C to the treated sample at 100 $^{o}$C is also observed although the treated sample at 300 $^{o}$C may be not BiOI since a heating treatment allowed the oxygen and iodine addition and subtraction. It may be $Bi_7O_9I_3$. The annealing treatment can lead to the distortion of BiOI structure due to the more bismuth and oxygen contained in the BiOI lattice crystal [29]. Some researchers noticed that it is difficult to distinguish between BiOI and $Bi_7O_9I_3$ because both materials have similar pattern and composition in their XRD patterns [26]. The annealed material at 300 $^{o}$C is also not $Bi_4O_5I_2$ [28]. The similar binding energy in the Bi and I region of BiOI and $Bi_7O_9I_3$ [32] makes those materials are difficult to differentiate by their XPS spectra. However, it is found that d-spacing value (0.280 nm) of this BiOI is matched to the reported work by Ren and co-workers [33], and the value for d-spacing of the treated sample at 300 $^{o}$C (0.285 nm) is near from the TEM d-spacing material for $Bi_7O_9I_3$ (0.286 nm) [34].

The average crystal size value of annealed BiOI at 100, 200, and 300 $^{o}$C also was calculated using the Debye-Scherrer equation, $L = K\lambda/\beta Cos\theta$, which represent to the crystallite size (L); constant (K, 0.9); wavelength of Cu (λ, 0.154 nm), full width at half maximum, FWHM (β, in radian); and Bragg angle (θ). The calculated average crystallite size was 29.97 nm; 33.06 nm;

27.42 for the annealed materials at 100, 200, and 300 $^{o}$C. Therefore, it is noticed that the heating process had an impact on crystal size distribution [35].

XRD patterns of the annealed BiOI at 450 and 550 $^{o}$C confirm for the character of $Bi_5O_7I$ and β-$Bi_2O_3$ crystals. $Bi_5O_7I$ crystal planes were assigned to the (001); (312); (004); (204); (020); and (316) at 2θ around 7.7$^{o}$; 28.2$^{o}$; 31.09$^{o}$; 33.02$^{o}$; 33.4$^{o}$; and 53.6$^{o}$ by referring to the JCPDS card no. 00-40-0548. Fig. 5.1 also informs the peaks (201) and (220) at 2θ around 27.9$^{o}$; and 32.6$^{o}$ correspond to the tetragonal β-$Bi_2O_3$ for the annealed sample at 550 $^{o}$C. It is matched to the data in the JCPDS card no. 00-27-0050 and previous research [36]. Moreover, the $Bi_5O_7I$ pattern is matched to the reported research [37]. The proposed reaction for BiOI reaction with oxygen is shown in the Eq. 5.1-5.3.

$$7BiOI + O_2 \rightarrow Bi_7O_9I_3 + 2I_2 \quad (5.1)$$

$$5Bi_7O_9I_3 + 2O_2 \rightarrow 7Bi_5O_7I + 4I_2 \quad (5.2)$$

$$4Bi_5O_7I + O_2 \rightarrow 10Bi_2O_3 + 2I_2 \quad (5.3)$$

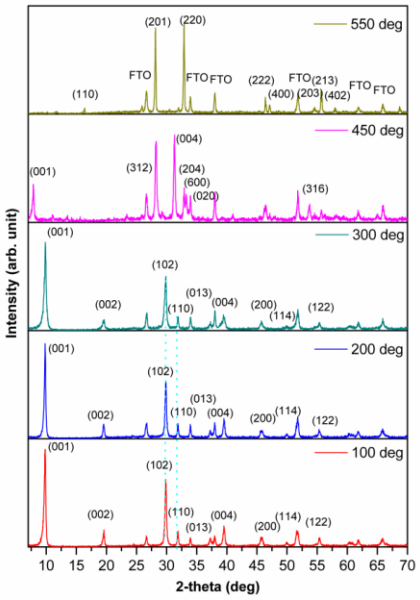


**Figure 5.1.** XRD pattern of annealed BiOI at several temperatures: 100; 200; 300; 450; and 550 $^{o}$C.

### 5.3.2. Raman analysis

Fig. 5.2 shows the results of Raman analysis. The vibration peak of Bi-I is notated to the Eg stretching which appears in 147-149 $cm^{-1}$ [38,39]. This information is confirmed from the annealed BiOI at 100 and 300 $^{o}C$. After the samples were annealed at a higher temperature, the Eg mode of Bi-I could shift to the higher frequency, like for $Bi_4O_5I_2$ and $Bi_5O_7I$ characters. It is also same as the reported work by Liu and co-worker [40]. Annealing treatment of BiOI at 550 $^{o}C$ resulted in the peak signals around 280-350 $cm^{-1}$ and 445-485 $cm^{-1}$ which closed to the character of β-$Bi_2O_3$ [41].

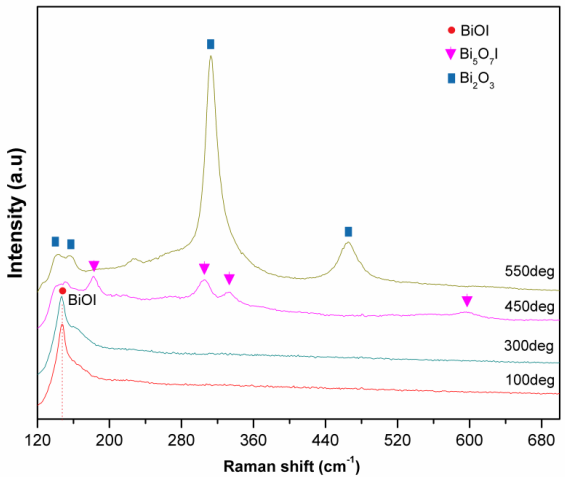


**Figure 5.2.** Raman spectra of annealed BiOI at a different temperature: 100; 300; 450; and 550 $^{o}C$.

## 5.4. Morphology analysis

Figure 5.3 depicts the SEM images of some annealed BiOI. It is obviously seen that there is no significant difference in the shape of annealed BiOI at 100 and 300 $^{o}C$ in Fig. 5.3A and 5.3B. Here, the obtained sheet-like material may be influenced by the condition during the synthesis process. BiOI growth can be affected by the acidity of solution which has an impact on the different facet of BiOI. The BiOI (001) facet growth can be caused by the less amount of water added to the precursor solution [42,43].

Next, in Fig. 5.3C, it can be seen that the material is composed by irregular nanosheet with some pores appeared in the surface. This image is nearly same as the synthesized $Bi_5O_7I$ by Yang and co-workers [30]. The annealed sample at 550 $^oC$ shows the biggest material like a dumbbell. The same morphology of this dumbbell-like material is also reported for β-$Bi_2O_3$ [36]. The annealing treatment may allow the shrinkage process in the materials due to the deiodination and oxygen incorporation like in the copper nitride material [44].

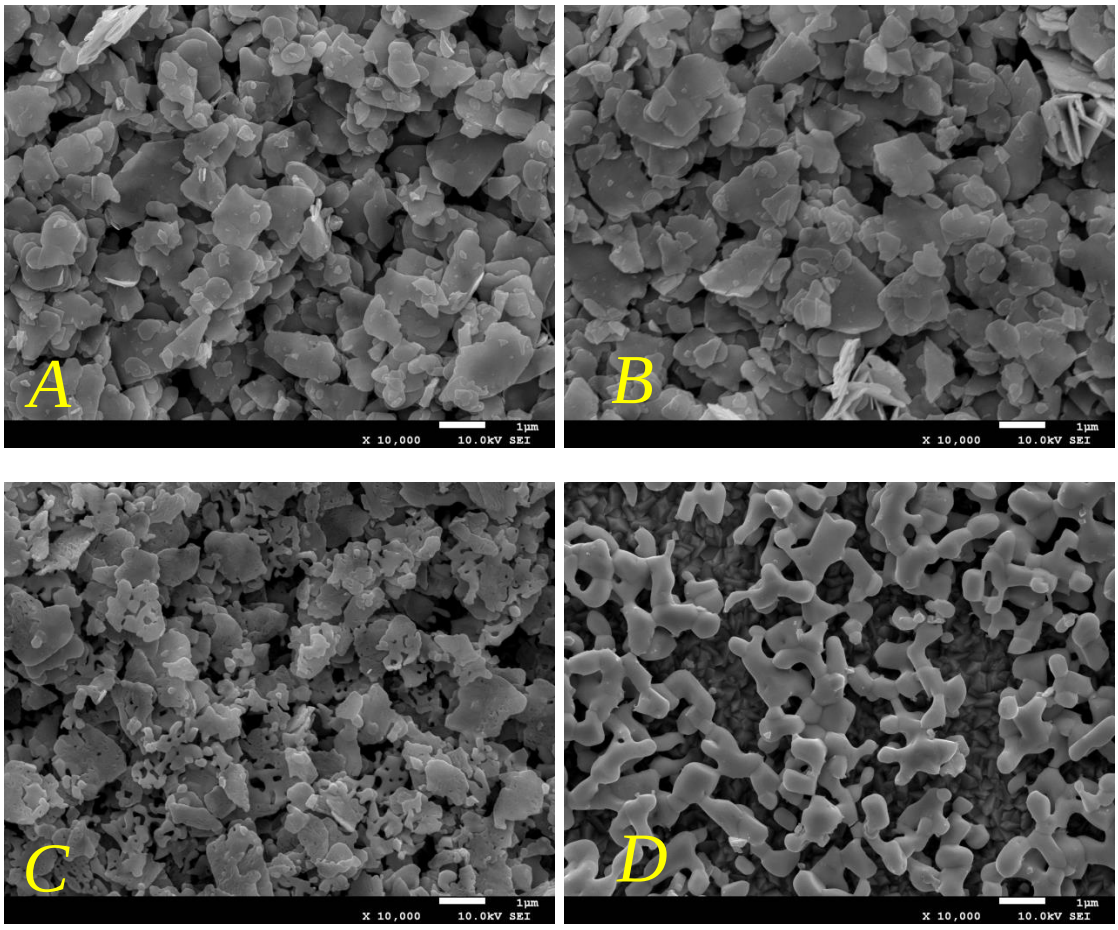


**Figure 5.3.** SEM images of annealed BiOI at a different temperature: 100 (A); 300 (B); 450 (C); 550 $^oC$ (D), and the higher magnification image of the annealed sample at 100 (E) and 300 $^oC$ (F).

## 5.5. Optical study

Fig. 5.4A shows the absorbance spectra of annealed BiOI materials from 100 to 550 $^{o}$C. The absorbance was calculated from the equation: $A = 1 - (T + R)$ [45]. It was noticed that the annealing treatment caused the blue-shift in its absorption behavior. The bandgap energy of bismuth-based materials can be calculated by the Tauc plot equation [46]. The indirect bandgap calculation for annealed BiOI is displayed in Figure 5.4B which shows the calculated bandgap energy of annealed BiOI at 100, 200, 300, 450, and 550 $^{o}$C as BiOI, BiOI, $Bi_7O_9I_3$, $Bi_5O_7I$, and $Bi_2O_3$ are 1.76; 1.77; 1.84; 2.18; 2.11. The data are in line with the calculated BiOI from the previous reports [26,47]. The bandgap energy of $Bi_5O_7I$ was slightly higher than $Bi_2O_3$ [48], and for β-$Bi_2O_3$, which was 2.15 eV [49]. While the deiodination results in the blue-shift absorption, in contrary, the oxygen-deficient in the BiOI structure may cause a redshift response for its absorption behavior [50].

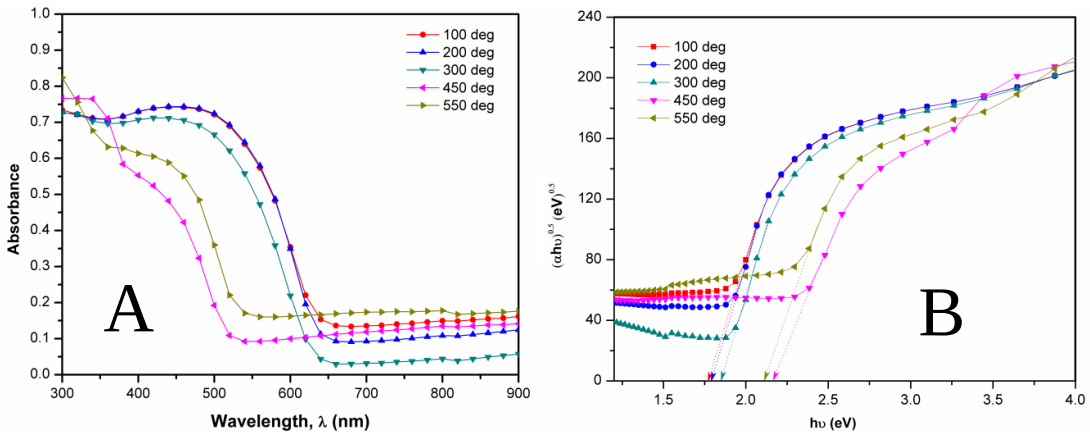


**Figure 5.4.** Absorbance spectra (A) and Tauc plot (B) of annealed BiOI at different temperature.

## 5.6. Photovoltaic test

Fig. 5.5A illustrates the prepared photovoltaic cells contained BiOI and its family in this work and Fig. 5.6A shows the resulted I-V tests. A short-circuit current (Jsc) and open-circuit voltage (Voc) trend on the annealing temperature of BiOI is displayed in Fig. 5.6B. The increase

in the temperature up to 300 $^{o}$C can result in the increasing of Jsc and Voc which is shown in the Fig. 5.6B. The wider light absorption may be responsible to reach the better Jsc which is influenced the light-harvesting ability [51]. Grain size, internal resistance, film quality, charge transfer model, and electron mobility may also have an impact on the Jsc.

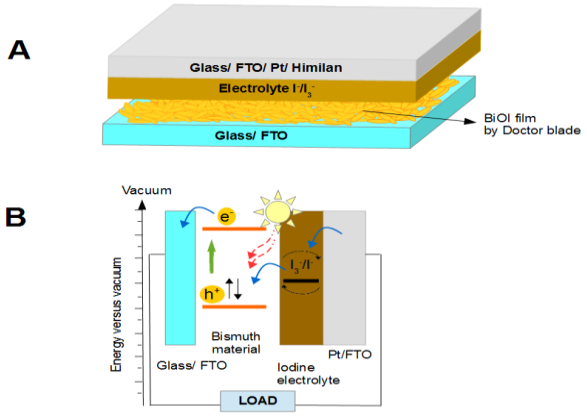


**Figure 5.5.** Device structure (A) and band structure illustration of annealed BiOI in the different temperature (B).

The annealed material at 300 $^{o}$C shows the best performance in comparison to the other annealed materials with the Jsc 0.438 mA/cm$^2$. Sample at 300 $^{o}$C may have the bigger surface area for better contact with liquid electrolyte material. This phenomenon is likely to happen in the $TiO_2$ porous-based solar cell. However, unfortunately, all of the Jsc values in this report were lower than the reported BiOI solar cell [52]. It may be caused by the bulky structure, different thickness, and different properties of material. Nevertheless, it is interesting to note that $Bi_7O_9I_3$ had better the photovoltaic activity in comparison to its parent BiOI which is similar to the photocatalytic behavior of $Bi_7O_9I_3$ [1,26,29]. It is expected that if a better quality of BiOI and its family are used, the cell performance may become higher than these results. Also, it can be suggested to apply the bismuth oxyiodides and its derivations, like $Bi_7O_9I_3$ for the absorber with the suitable hole and electron transport layer like in the reported device structure [11].

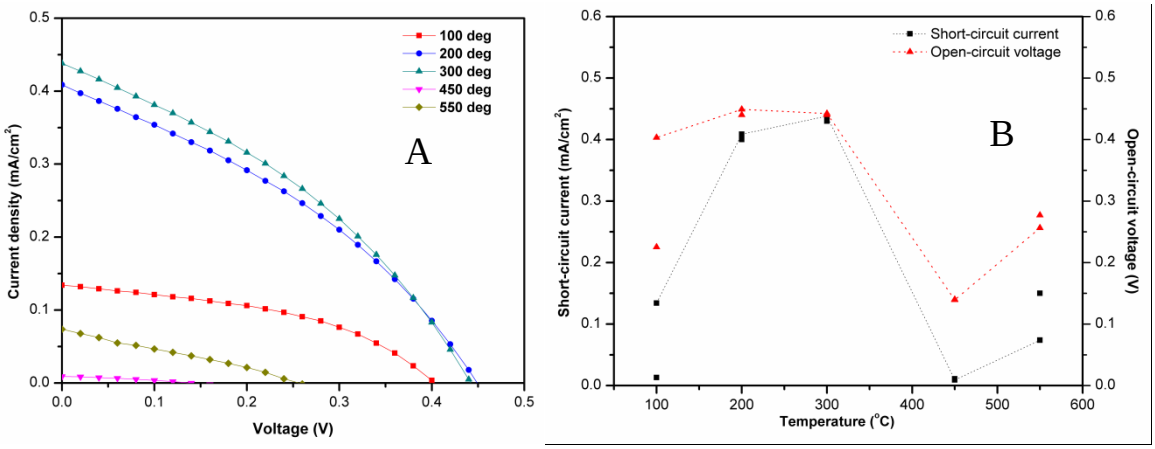


**Figure 5.6.** I-V curve of annealed BiOI at different temperature (A), and short-circuit current and open-circuit voltage trend as the function of temperature (B).

## 5.7. Conclusions

The annealing treatment in BiOI had the effect on the structural, morphological, and optical properties. Therefore, they have the different character for their photovoltaic cell performance. The annealed BiOI at 300, 450, and 550 $^{o}$C caused the conversion of BiOI to $Bi_7O_9I_3$, $Bi_5O_7I$, and β-$Bi_2O_3$. Heated material at 300 $^{o}$C as $Bi_7O_9I_3$ reached the best photovoltaic cell performance in comparison to other materials. The resulted photovoltaic trend for BiOI derivation, especially for $Bi_7O_9I_3$ is in line with its performance for photocatalytic reaction. Therefore, it can be suggested to apply $Bi_7O_9I_3$ as the absorber for photovoltaic device which uses the suitable hole and electron transport layer.

## 5.8. References

[1] W.W. Lee, C.S. Lu, C.W. Chuang, Y.J. Chen, J.Y. Fu, C.W. Siao, C.C. Chen, *RSC Adv*. 5 (2015) 23450–23463.

[2] R. He, J. Zhang, J. Yu, S. Cao, *J. Colloid Interface Sci.* 478 (2016) 201–208.

[3] X. Zhang, L. Zhang, *J. Phys. Chem. C* 114 (2010) 18198–18206.

[4] J. Niu, P. Dai, Q. Zhang, B. Yao, X. Yu, *Appl. Surf. Sci.* 430 (2018) 165–175.

[5] X. Zhang, L. Zhang, T. Xie, D. Wang, *J. Phys. Chem. C* 113 (2009) 7371–7378.

[6] J. Cao, B. Xu, B. Luo, H. Lin, S. Chen, *Catal. Commun.* 13 (2011) 63–68.

[7] J. Hou, K. Jiang, M. Shen, R. Wei, X. Wu, F. Idrees, C. Cao, *Sci. Rep.* 7 (2017) 11665.

[8] R. Hao, X. Xiao, X. Zuo, J. Nan, W. Zhang, *J. Hazard. Mater.* 209–210 (2012) 137–145.

[9] H. Cheng, B. Huang, Y. Dai, X. Qin, X. Zhang, *Langmuir* 26 (2010) 6618–6624.

[10] A. Han, H. Zhang, G.K. Chuah, S. Jaenicke, *Appl. Catal. B Environ.* 219 (2017) 269–275.

[11] R.L.Z. Hoye, L.C. Lee, R.C. Kurchin, T.N. Huq, K.H.L. Zhang, M. Sponseller, L. Nienhaus, R.E. Brandt, J. Jean, J.A. Polizzotti, A. Kursumović, M.G. Bawendi, V. Bulović, V. Stevanović, T. Buonassisi, J.L. MacManus-Driscoll, *Adv. Mater.* 29 (2017) 1–10.

[12] L. Wang, W.A. Daoud, *Appl. Surf. Sci.* 324 (2015) 532–537.

[13] S. Sfaelou, D. Raptis, V. Dracopoulos, P. Lianos, *RSC Adv.* 5 (2015) 95813–95816.

[14] Y. Zhang, Q. Pei, J. Liang, T. Feng, X. Zhou, H. Mao, W. Zhang, Y. Hisaeda, X.M. Song, *Langmuir* 31 (2015) 10279–10284.

[15] K. Wang, F. Jia, L. Zhang, *Mater. Lett.* 92 (2013) 354–357.

[16] K. Wang, F. Jia, Z. Zheng, L. Zhang, *Electrochem. Commun.* 12 (2010) 1764–1767.

[17] Y. Zhang, Y. Li, W. Sun, C. Yuan, B. Wang, W. Zhang, X.M. Song, *Langmuir* 33 (2017) 12065–12071.

[18] Y. Lei, G. Wang, S. Song, W. Fan, M. Pang, J. Tang, H. Zhang, *Dalt. Trans.* 39 (2010) 3273–3278.

[19] X. Xiao, W.-D. Zhang, *J. Mater. Chem.* 20 (2010) 5866–5870.

[20] Y. Long, Q. Han, Z. Yang, Y. Ai, S. Sun, Y. Wang, Q. Liang, M. Ding, *J. Mater. Chem. A* 6 (2018) 13005–13011.

[21] C.J. Meledandri, J.K. Stolarczyk, S. Ghosh, D.F. Brougham, *Langmuir* 24 (2008) 14159–14165.

[22] A. Demortière, P. Panissod, B.P. Pichon, G. Pourroy, D. Guillon, B. Donnio, S. Bégin-Colin, *Nanoscale* 3 (2011) 225–232.

[23] F.B. Effenberger, R.A. Couto, P.K. Kiyohara, G. Machado, S.H. Masunaga, R.F. Jardim, L.M. Rossi, *Nanotechnology* 28 (2017) 115603.

[24] R. Hufschmid, H. Arami, R.M. Ferguson, M. Gonzales, E. Teeman, L.N. Brush, N.D.

Browning, K.M. Krishnan, *Nanoscale* 7 (2015) 11142–11154.

[25] W. Baaziz, B.P. Pichon, S. Fleutot, Y. Liu, C. Lefevre, J.-M. Greneche, M. Toumi, T. Mhiri, S. Begin-Colin, *J. Phys. Chem. C* 118 (2014) 3795–3810.

[26] M. Long, P. Hu, H. Wu, Y. Chen, B. Tan, W. Cai, *J. Mater. Chem. A* 3 (2015) 5592–5598.

[27] X. Xiao, C. Liu, R. Hu, X. Zuo, J. Nan, L. Li, L. Wang, *J. Mater. Chem.* 22 (2012) 22840.

[28] J. Xia, M. Ji, J. Di, B. Wang, S. Yin, M. He, Q. Zhang, H. Li, *J. Alloys Compd.* 695 (2017) 922–930.

[29] X. Xiao, W. De Zhang, *RSC Adv.* 1 (2011) 1099–1105.

[30] J. Yang, L. Xu, C. Liu, T. Xie, *Appl. Surf. Sci.* 319 (2014) 265–271.

[31] H. Cheng, B. Huang, J. Lu, Z. Wang, B. Xu, X. Qin, X. Zhang, Y. Dai, *Phys. Chem. Chem. Phys.* 12 (2010) 15468.

[32] D. Zhang, F. Wang, S. Cao, X. Duan, *RSC Adv.* 8 (2018) 5967–5975.

[33] X. Ren, J. Yao, L. Cai, J. Li, X. Cao, Y. Zhang, B. Wang, Y. Wei, *New J. Chem* 43 (2019) 1523.

[34] S.Y. Chou, C.C. Chen, Y.M. Dai, J.H. Lin, W.W. Lee, *RSC Adv.* 6 (2016) 33478–33491.

[35] M. Khalid, M. Mujahid, S. Amin, R.S. Rawat, A. Nusair, G.R. Deen, *Ceram. Int.* 39 (2013) 39–50.

[36] J. Yang, T. Xie, C. Liu, L. Xu, *Materials (Basel).* 11 (2018) 1359.

[37] H. Wang, L. Xu, C. Liu, Y. Lu, Q. Feng, T. Wu, R. Wang, *Nanomaterials* 9 (2019) 118.

[38] Y. Park, Y. Na, D. Pradhan, B.-K. Min, Y. Sohn, *CrystEngComm* 16 (2014) 3155–3167.

[39] M. Fang, H. Jia, W. He, Y. Lei, L. Zhang, Z. Zheng, *Phys. Chem. Chem. Phys.* 17 (2015) 13531–13538.

[40] C. Liu, X.J. Wang, *Dalt. Trans.* 45 (2016) 7720–7727.

[41] C. Díaz-Guerra, P. Almodóvar, M. Camacho-López, S. Camacho-López, J. Piqueras, *J. Alloys Compd.* 723 (2017) 520–526.

[42] J. Lu, J. Wu, W. Xu, H. Cheng, X. Qi, Q. Li, Y. Zhang, Y. Guan, Y. Ling, Z. Zhang, *Mater. Lett.* 219 (2018) 260–264.

[43] R. He, J. Zhang, J. Yu, S. Cao, *J. Colloid Interface Sci.* 478 (2016) 201–208.

[44] Y. Du, R. Huang, R. Song, L.B. Ma, C. Liu, C.R. Li, Z.X. Cao, *J. Mater. Res.* 22 (2007) 3052–3057.

[45] E. Brugnoli, O. Björkman, *Photosynth. Res.* 32 (1992) 23–35.

[46] H. Cheng, B. Huang, Y. Dai, X. Qin, X. Zhang, *Langmuir* 26 (2010) 6618–6624.

[47] F.Q. Ma, J.W. Yao, Y.F. Zhang, Y. Wei, *RSC Adv*. 7 (2017) 36288–36296.

[48] S. Sun, W. Wang, L. Zhang, L. Zhou, W. Yin, M. Shang, *Environ. Sci. Technol.* 43 (2009) 2005–2010.

[49] M. Schlesinger, M. Weber, S. Schulze, M. Hietschold, M. Mehring, *ChemistryOpen* 2 (2013) 146–55.

[50] Y. Huang, H. Li, M.-S. Balogun, W. Liu, Y. Tong, X. Lu, H. Ji, 6 (2014) 22920−22927.

[51] Z.-S. Wang, Y. Cui, K. Hara, Y. Dan-oh, C. Kasada, A. Shinpo, *Adv*. *Mater.* 19 (2007) 1138–1141.

[52] A.A. Putri, S. Kato, N. Kishi, T. Soga, *J. Sci. Adv*. *Mater. Devices* 4 (2019) 116–124.

# CHAPTER 6

# $TiO_2/Bi_5O_7I$ COMPOSITE FILMS FOR PHOTOVOLTAIC DEVICE

## 6.1. Introduction

The consumption of fossil fuels for fulfilling the global energy demand has led to many environmental problems. Since the electricity generation through solar cell based on the DSSC has been established [1], the research on the photovoltaic devices development is still being an interesting topic to date. Solar cell is considered to be a promising source to generate electricity because it is environmentally benign and it utilizes the materials which are abundant on earth. Moreover, it is important to note that solar power is renewable resources of energy, not like fossil fuels which is non-renewable energy resources.

In order to get the better performance of photovoltaic devices through DSSC, there are many works have been reported which have focused on the photoanode modification since it is considered being the major component in DSSC. Photoanode should have good transparency and good visible light absorption ability to maximize its performance. Regarding it, some efforts have been attempted. The films deposition technique modified with post-annealing treatment on the DSSC photoanode showed the improvement on the performance of $TiO_2$ and ZnO-based DSSC compared with unmodified photoanode [2–5]. Other works, the doping treatment in $TiO_2$ photoanode and $TiO_2$–organic material composite application for DSSC have been aimed for electrical transport properties modification which could achieved the better performance than undoped material and non-composite films [6,7].

Structural and composition modification of semiconductors also have affected the semiconductors' performance. By utilizing the dopant in the semiconductor materials, the

catalytic activity of semiconductor materials improved owing to the doping process. $TiO_2$ can be doped easily with several elements, such as copper [8], nitrogen [9], chromium [10], iron [11], and carbon [12]. Due to the structural modification by dopant insertion, the band gap energy of doped material changes and it can be one of factors to increase the open-circuit voltage [8]. By involving other oxide compounds like $Nb_2O_5$, the photoanode of DSSC can be constructed from composite material which causes the improvement on the solar cell performances as the consequence of the changing in its electron transport. Furthermore, the increasing in the dye adsorption ability related to the increase in the light harvesting which resulted in the better performance of DSSC [13].

$Bi_5O_7I$ is one of the bismuth oxyiodides (BiOI) family which can be synthesized directly by oxidation of BiOI through calcination [14] and the pH adjustment in the synthesis process from its precursors [15]. $Bi_5O_7I$ has exhibited the great work as photocatalyts [16–18]. This material could perform an excellent work on the photodegradation of organic pollutants under radiation of visible light for more than 400 nm [16]. Furthermore, $Bi_5O_7I$ could be composited with other materials to improve its performance on photocatalytic reaction [19,20]. Due to the fact that $Bi_5O_7I$ semiconductor has good performance in photocatalytic reaction, it may be worth to combine $Bi_5O_7I$ and $TiO_2$ as the photoanode in DSSC. Here, the comparison between composite $TiO_2/Bi_5O_7I$ for DSSC under the dye loading and without dye usage will be discussed.

Through this work, the DSSC made from the composite $Bi_5O_7I/TiO_2$ can be studied. The effect of $Bi_5O_7I$ addition to the $TiO_2$ semiconductor for DSSC application with N719 dye and without using the dye also has been screened. To date, there is no study on the $Bi_5O_7I$ as the component for photovoltaic devices. By this result it can be pointed that the bismuth-based material has a chance to be optimized for the future photovoltaic device. It has been known that

by using $Bi_5O_7I/TiO_2$ composite materials, the open-circuit voltage of DSSC increased slightly along with the improvement of $Bi_5O_7I$ proportion. Furthermore, by involving ratio 1:4 in $Bi_5O_7I:TiO_2$ as the photoanode in DSSC, it achieved the best efficiency up to 1.9% in comparison to the $TiO_2$-based device. It is also interesting to note that the $Bi_5O_7I$ devices showed the better performance than $Bi_2O_3$-based material for photoelectrochemical application [21–23].

## 6.2. Synthesis and fabrication of BiOI films

BiOI powder was prepared by the grinding of $Bi(NO_3)_3.5H_2O$ and KI for 15 minutes. The black mixed-solid precursor as a result of the mixing process then was hydrolyzed in water solvent for 5 h through stirring treatment at room temperature. The orange solid BiOI as the product in this process was washed in ethanol and deionized water for several times. To obtain the composite materials, different ratio of BiOI and $TiO_2$ in ethanol was prepared to result in the $BiOI:TiO_2$ ratio at 0:1; 1:16; 1:8; 1:4; 1:2; and 1:0. Each sample was dispersed vigorously using a homogenizer (Sonic VCX-130) for 15 minutes. After the paste of $BiOI:TiO_2$ was obtained, the slip casting method was utilized to prepare the film onto cleaned FTO glass substrates. The obtained films were annealed at 450 $^oC$ for 1h to get $Bi_5O_7I/TiO_2$ composites with ratio $Bi_5O_7I:TiO_2$ 0:1; 1:16; 1:8; 1:4; 1:2; and 1:0. The thickness of each film was ~6 μm which was measured via cross-sectional SEM image of samples. The heating treatment at 450 $^oC$ allows the transformation from BiOI to $Bi_5O_7I$. Finally, $Bi_5O_7I/TiO_2$ composite films could be obtained.

X-Ray Diffraction (XRD, RINT-2100 diffractometer) and Raman Spectrometer (JASCO NRS-2100) have been utilized to study the structural characters of prepared films. The XRD measurement involved the Cu target with Cu Kα radiation at 1.5408 Å and it has the X-ray tube voltage and current at 40 kV and 30 mA, respectively. The morphology of films was observed by FESEM JEOL JSM-7100F and the optical properties were studied by UV-Visible

spectrophotometer (JASCO 670 UV). Last, the solar cell performance was studied by I-V characteristics measurement using solar cell simulator under white light illumination of standard radiation (AM 1.5G, 100 mW/cm$^2$).

During the work, the photovoltaic devices were prepared adapting from dye-sensitized solar cell (DSSC) model as the structure: FTO-$Bi_5O_7I/TiO_2$ as photoanode and Pt-FTO/glass covered with polymer film (Himilan, 50 μm) as counter electrode. $I^-/I_3^-$ solution (Iodolyte AN 50, Solaronix) was used as electrolyte in the experiment. The photoanode was soaked into ethanolic solution of 0.5 mM N719 dye (Ruthenium-525 bis TBA, Solaronix) for 18 h. Before testing the solar cell performance, the photoanode was cleaned with methanol and dried in $N_2$ flow. 0.16 cm$^2$ of active area was designed to measure the I-V character of each film. The $TiO_2/Bi_5O_7I$ composite cells were applied for DSSC and the cell without using the dye.

## 6.3. Structural analysis

To study the structural property of prepared films, XRD patterns of $Bi_5O_7I/TiO_2$ composite films are displayed in Figure 6.1. After annealing treatment at 450 $^oC$ for each film, the character of $Bi_5O_7I$ and $TiO_2$ can be observed in the film composite. Based on the JCPDS card no. 00-40-0548, some peaks which represent for $Bi_5O_7I$ are found, like (312) and (004) crystal planes at 2θ around 28.2$^o$ and 31.2$^o$, respectively. Peak (101) for $TiO_2$ anatase also arises in 2θ around 25.4$^o$ which is in line to the literature [24]. Due to the different ratio, the peak intensity of each diffractogram in Figure 6.1 is different.

The XRD patterns were depicted from the mixing between $TiO_2$ and $Bi_5O_7I$ by the different ratio of $Bi_5O_7I$:$TiO_2$, namely 1:8; 1:4; and 1:2. The more amount of material can show the higher intensity in their XRD patterns. For example, the more concentration of $Bi_5O_7I$ in the film can be reflected by the higher peak of this material character in the diffractogram as shown in Fig. 6.1.

The crystal grain of $Bi_5O_7I$ can be calculated using the Debye-Scherrer in Eq. 2.2 which obtained 31.25 nm as the average value of $Bi_5O_7I$ crystal size in pure $Bi_5O_7I$.

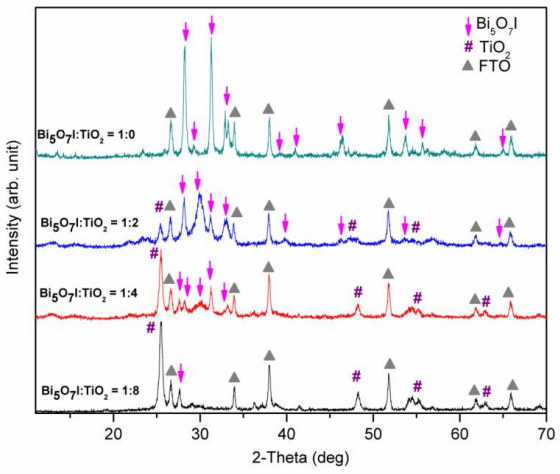


**Fig. 6.1** XRD patterns of $TiO_2/Bi_5O_7I$ composite in the different ratio of $Bi_5O_7I$:$TiO_2$.

Raman spectra in Figure 6.2 show that $Bi_5O_7I$ peak in the composited film is covered with $TiO_2$ peak because the peaks of those materials are closer. It is difficult to give an exact label to the assigned $Bi_5O_7I$ peak since it showed an overlapping peak. Bi-I vibration mode appears in Raman shift near from 150 $cm^{-1}$, while $TiO_2$ also has a peak character near from 140 $cm^{-1}$ of Raman shift. However, it is observed that $TiO_2$ peak in the composited material has the wider peak in comparison to the pure $TiO_2$. Hence, it can be assumed that the bismuth incorporation might happen into $TiO_2$ crystal structure to form titanium oxide and bismuth species like in the –Ti-O-Fe-Ti-O- in the $Fe_2O_3/TiO_2$ composites [25]. Then, the Bi-I and Bi-O bond characters are difficult to observe in the Raman spectra. This is also similar to the circumstance at the reported works for $TiO_2$ composite with iron and copper compounds [25,26].

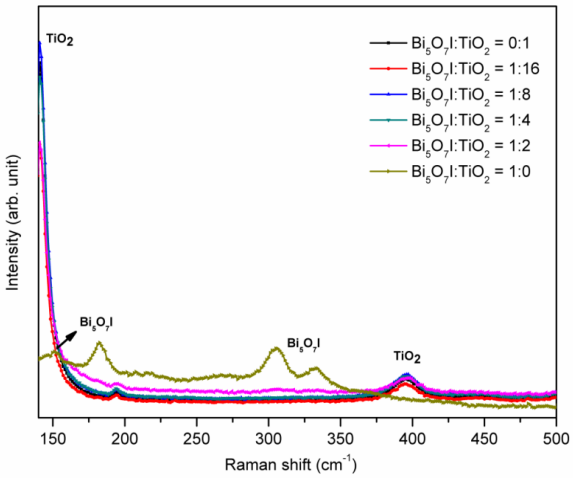


**Fig. 6.2** Raman spectra of $TiO_2/Bi_5O_7I$ composite in the different ratio of $Bi_5O_7I$:$TiO_2$.

The Raman patterns confirm the anatase $TiO_2$ and $Bi_5O_7I$ films which are similar to the previous reports [16,27]. Besides the peak appears in the wavenumber around 150 $cm^{-1}$, it can also be observed the peak of $Bi_5O_7I$ near from 180 $cm^{-1}$ and 300 $cm^{-1}$ in Raman spectra. It may come from the contribution of Bi-O bond based on the information that Bi-O stretches in oxide bismuth materials can be found below 600 $cm^{-1}$ [28]. The $Bi_5O_7I$ spectra is also in line to those Raman patterns in the Jiang and co-workers' and Liang and co-workers' works [29,30]. It is obviously seen that Raman spectra of pure $Bi_5O_7I$ is different from the composite $Bi_5O_7I/TiO_2$ since it does not contain $TiO_2$. The conversion of BiOI as an initial material in this work to $Bi_5O_7I$ may be caused by the heating treatment together with $TiO_2$ which can take place due to the oxidation reaction. The reaction occurred as it is shown in the equation 6.1 and 6.2.

$$7BiOI + O_2 \rightarrow Bi_7O_9I_3 + 2I_2 \quad (6.1)$$

$$5Bi_7O_9I_3 + 2O_2 \rightarrow 7Bi_5O_7I + 4I_2 \quad (6.2)$$

Heating treatment allows the oxygen addition to BiOI and deiodination in order to produce bismuth and oxygen-rich material with iodine deficient. Hence, the vibrational modes of Bi-I

shifts from the original position in BiOI (147 $cm^{-1}$) [31] to the higher frequency which is more than 150 $cm^{-1}$. This character is similar to the reported work [18].

## 6.4. Morphology analysis

Figure 6.3 displays SEM analysis images of the composite films in the different ratio of $Bi_5O_7I$ and $TiO_2$. There is no change in the morphology of $TiO_2$ and $Bi_5O_7I$ among the prepared samples. $TiO_2$ has the particulate morphology and $Bi_5O_7I$ has the sheet shape both in the composited and pure materials. However, the more percentage $Bi_5O_7I$ contained in the sample is proven by the more quantity of $Bi_5O_7I$ in the SEM images. In this work, $Bi_5O_7I$ in Fig. 6.3C has the sheet-like material which is bigger than porous $TiO_2$ P25. Normally the bismuth-based material has the morphology which based on the 2D structures, like flake or sheet shape. Moreover, in the higher magnification image of composite $Bi_5O_7I/TiO_2$ (Figure 6.3D), it is clearly viewed that the $Bi_5O_7I$ with 76 nm-thick thickness of sheet tends to have the pores in its surface like circles with almost same size.

The appeared pores in the surface of bismuth-based material may be a common effect in the calcination treatment of BiOI at temperature for more than 450 $^oC$. The circumstance of $Bi_5O_7I$ is also similar to the previous report of $Bi_5O_7I$ nanosheet [16]. The high temperature in calcination allows the oxygen insertion and iodine lost from the BiOI structure. Then, the space of iodine as the counter anion in this material may convert into pores. This illustration may be same as the nanopores conversion which is occurred in the cobalt materials due to the dehydration [32].

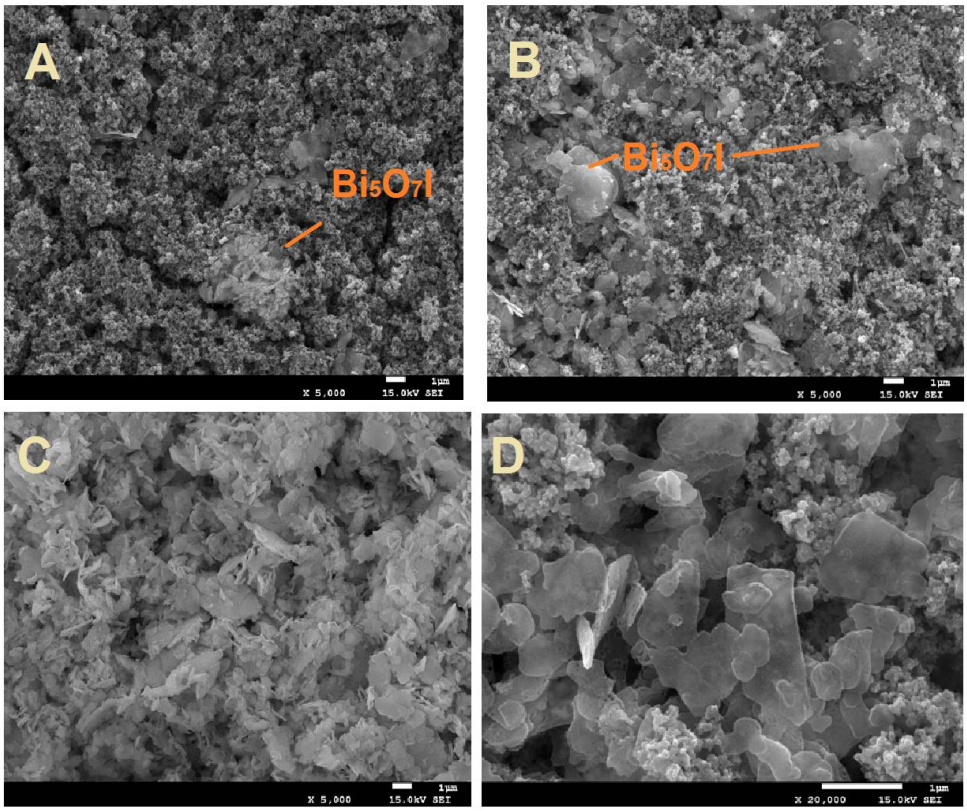


**Fig. 6.3** SEM images of $TiO_2/Bi_5O_7I$ composite in the different ratio of $Bi_5O_7I$:$TiO_2$ 1:8 (A); 1:4 (B); 1:0 (C); and 1:4 sample for the higher magnification (D).

## 6.5. Optical study

To study the response of semiconductor material with light radiation due to the $Bi_5O_7I$ addition on $TiO_2$, the absorbance spectra of composite $Bi_5O_7I/TiO_2$ is shown. Absorbance value was calculated from the transmittance and reflectance value of material, following the equation: $1 = A + T + R$, whereas $A, T, R$ are absorbance, transmittance, and reflectance, respectively. In Fig. 6.4A, it can be clearly seen that due to the $Bi_5O_7I$ composition in the composite material, there is a red shift in its absorbance spectra. Since pure $Bi_5O_7I$ has the response in the visible light up to the band edge near from 480 nm, it causes the longer visible light absorption for the more percentage of $Bi_5O_7I$ in $Bi_5O_7I/TiO_2$ composite. Hence, it is interesting to note that $Bi_5O_7I$ can give a flavor in the $TiO_2$ composite although $Bi_5O_7I$ is not a dye compound.

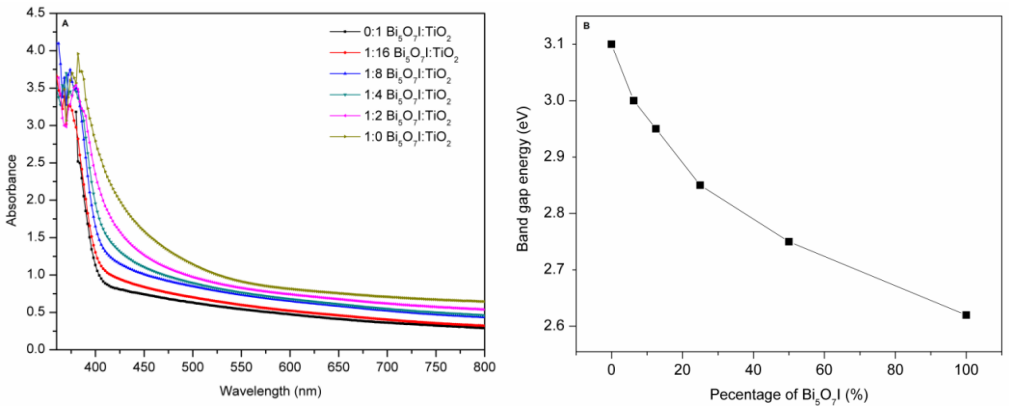


**Fig. 6.4** UV/Visible absorbance spectra (A) and band gap energy plot (B) of $TiO_2/Bi_5O_7I$ composite in the different ratio of $Bi_5O_7I$:$TiO_2$.

Band gap energy calculation for these composites films was determined based on the Tauc plot calculation [33]. Mostly, band gap energy of the bismuth-based materials is determined based on the indirect type [16]. By the Figure 4B, it is known that band gap energy decreases with the increase in the amount of $Bi_5O_7I$ in the samples. The different band gap energy may change the position of electronic bands of material which affects the performance on their photocatalytic and photovoltaic performances. Here, the band gap energy is shifted from 3.1 to 2.6 eV for ratio of $Bi_5O_7I$:$TiO_2$ from 0:1 to 1:0.

## 6.6. Photovoltaic study

First, study in the photovoltaic behavior for $TiO_2/Bi_5O_7I$ films was carried out without using N719 dye which the illustration of device is shown in the Fig. 6.5 and its I-V test result is displayed in Fig. 6.6. By this result, it is noticed that the $Bi_5O_7I$ usage has an effect on its photovoltaic performance. As the amount of this material increases, the ability in light harvesting also increases. Therefore, its Jsc will be higher as the impact of the higher visible light absorption. Comparing to the pure $TiO_2$ film in $Bi_5O_7I$:$TiO_2$ 0:1, the only $Bi_5O_7I$ photoanode exhibits the highest photovoltaic parameter due to its highest Jsc. In addition, the bigger size of

$Bi_5O_7I$ may have the light scattering effect to maximize its Jsc. Therefore, the PCE has doubled for the $Bi_5O_7I$ device.

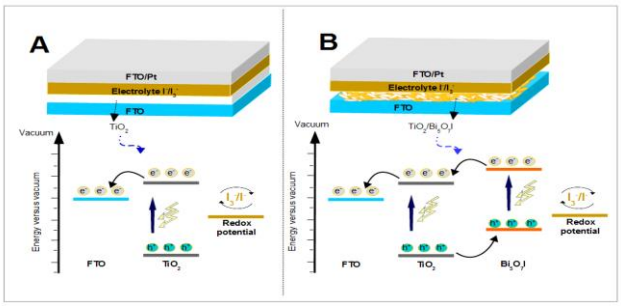


**Figure 6.5** The illustration of photovoltaic device structure (without dye) for $TiO_2$ (A) and $TiO_2/Bi_5O_7I$ (B).

The resulted composite material shows the quality improvement for photovoltaic device application as it indicated the slight increment in the open-circuit voltage value and a gradual increase of the short-circuit current.

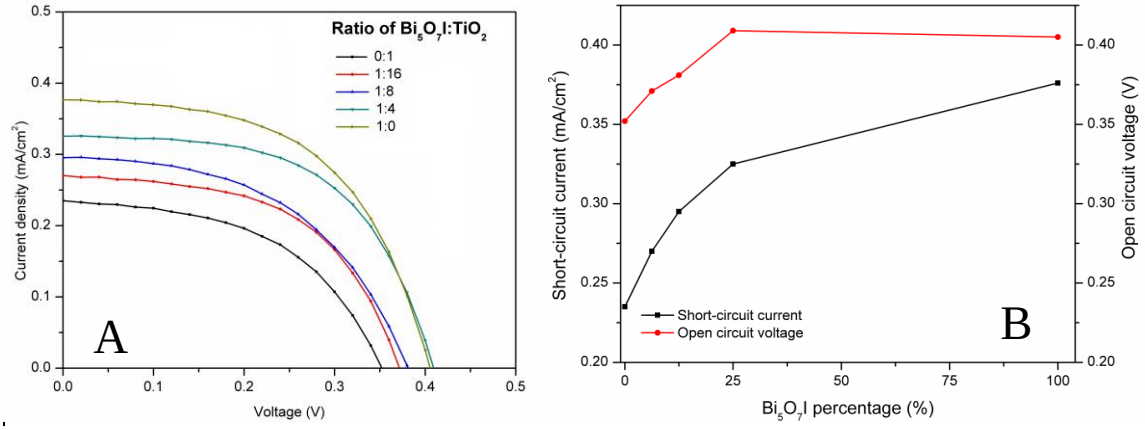


**Figure 6.6** I-V curve (A) and Jsc and Voc graph (B) of $TiO_2/Bi_5O_7I$ photovoltaic devices (without dye) in the different ratio of $Bi_5O_7I$:$TiO_2$.

Second, the IV test analysis was conducted by adapting the DSSC principle with dye adsorption. The device illustration is depicted in Fig. 6.7 and its I-V result is shown in Fig. 6.8. It can be seen that by using the composite materials contained $Bi_5O_7I$ with dye, it can result in the increase in short-circuit current (Jsc) and open-circuit voltage (Voc) values up to 7.286 $mA/cm^2$

and 0.624 V. The cell performance of composited material is higher than its single material for photoanode which up to 1.9%. From the $TiO_2$-based material, it only reaches for 1.1% of efficiency and after $Bi_5O_7I$ was added to the composite material, the efficiency increased up to 60% for $Bi_5O_7I$:$TiO_2$ with ratio 1:4.

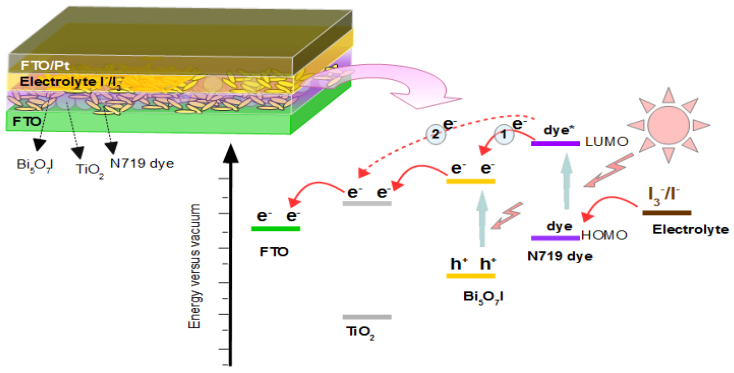


**Figure 6.7** Illustration of DSSC device structure for $TiO_2$/$Bi_5O_7I$ composite.

The Jsc increment is caused by the higher ability of composited material in light harvesting compared to $TiO_2$ only. Composited materials can have the longer absorption in visible spectral range [34]. The larger particles with smaller surface area also have the advantages on DSSC since those materials cause the scattering effect. This effect can enhance the photovoltaic performance. The scattering effect generates a light trapping effect which can be a role major for electricity production via DSSC. As a consequence, their Jsc values are being higher. $Bi_5O_7I$ seems to have this behavior and it promotes to be a promising material for collecting light in the composite photovoltaic device like the prepared photoanodes made from $TiO_2$ rutile-$ZrO_2$ and mixing of prepared $TiO_2$ particles via sol-gel method and $TiO_2$ P25 [35,36].

However, after higher amount of $Bi_5O_7I$ addition, the Jsc tends to be lower. The bigger size of $Bi_5O_7I$ may inhibit the dye adsorption ability in the photoanode which can reduce the light harvesting ability of $Bi_5O_7I$/$TiO_2$ composite in higher percentage of $Bi_5O_7I$. Nevertheless, it is

found that $Bi_5O_7I$ could make an interaction with the N719 dye and showed the positive IV curve response in its photovoltaic test. The dye loading in small amount of $Bi_5O_7I$ might be better than in the more $Bi_5O_7I$ since the more dye adsorption can increase the photons absorption in visible spectral range [37]. In addition, the bigger $Bi_5O_7I$ may reduce the contact effectivity between the photoanode and $I^-/I_3^-$ electrolyte since a good electron penetration will improve the electron transfer in the photovoltaic system which impacts on the Jsc increment [38]. Other factors which also can influence in the Jsc value are electron mobility, grain size, film quality, internal resistance, and charge transfer model. The increase in the ratio of $Bi_5O_7I$ in composite films can generate a slight increase in the Voc value. The higher ratio of $Bi_5O_7I$ might result in the Rsh value enhancement which has impact on its open-circuit voltage.

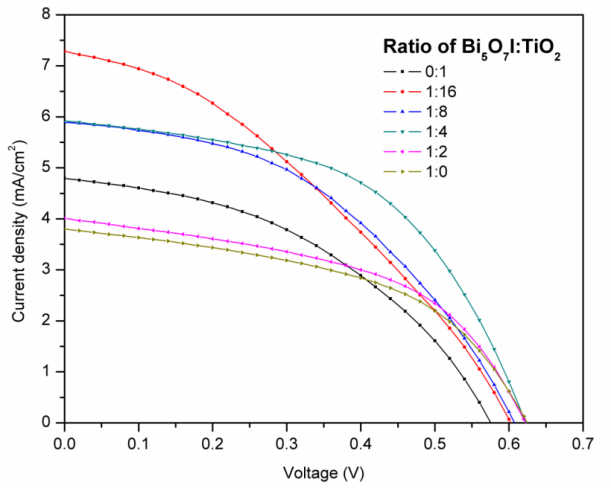


**Fig. 6.8** I-V curve of $TiO_2/Bi_5O_7I$ composite in the different ratio of $Bi_5O_7I$:$TiO_2$.

The performance of $TiO_2/Bi_5O_7I$ cell has been compared with the $TiO_2/Bi_2O_3$ cell and $TiO_2$/BiOI cell in the previous reports. Due to the different band gap energy among those bismuth materials, with the arrangement: BiOI < $Bi_5O_7I$ < $Bi_2O_3$, the short-circuit current also has the order list: $TiO_2$/BiOI > $TiO_2/Bi_5O_7I$ > $TiO_2/Bi_2O_3$ [23,39]. The light harvesting ability of those materials may be responsible to short-circuit current enhancement. Generally, the more

addition of $Bi_5O_7I$ to the films also has an impact on the open-circuit voltage (Voc). The new electronic structure due to the combination of $Bi_5O_7I$ and $TiO_2$ may be the reason to the Voc changing.

## 6.7. Conclusions

In this study, the $Bi_5O_7I/TiO_2$ composite films could be prepared by the annealing treatment of $BiOI/TiO_2$ at 450 $^oC$. Without using the dye, as the $Bi_5O_7I$ weight percentage increased, it could induce the red-shifting of composite materials which extended the visible absorption wavelength edge. Therefore, $Bi_5O_7I$ usage had the impact on its photovoltaic properties and it achieved the better performance than the only $TiO_2$ film. By increasing the amount of $Bi_5O_7I$ in DSSC, it can be clearly observed that the Jsc increased resulted in the higher PCE value. A ratio 1:4 for $Bi_5O_7I$:$TiO_2$ had the best efficiency among the DSSC devices, which up to 1.9%. The changing in the film composition also could reveal the different Voc value which could be caused by the different electronic structure of semiconductor material in the photoanodes. For future, the $Bi_5O_7I$ condition can be upgraded to pursue the higher of solar cell performance.

## 6.8. References

[1] B.O. Regan, M. Gratzel, 353 (1991) 737–740.

[2] M.S.H. Choudhury, N. Kishi, T. Soga, *Jpn. J. Appl. Phys.* 55 (2016) 1–4.

[3] M.S.H. Choudhury, N. Kishi, T. Soga, *J. Alloys Compd.* 656 (2016) 476–480.

[4] M.S.H. Choudhury, N. Kishi, T. Soga, *2017 IEEE 44th Photovolt. Spec. Conf. PVSC 2017* (2017) 1–6.

[5] M.S. Haque Choudhury, N. Kishi, T. Soga, *Mater. Res. Bull.* 80 (2016) 135–138.

[6] M. Shamimul, H. Choudhury, S. Kato, N. Kishi, T. Soga, *Jpn. J. Appl. Phys.* 56 (2017).

[7] A.A. Abuelwafa, M.S.H. Choudhury, M. Dongol, M.M. El-Nahass, T. Soga, *J. Mater. Sci. Mater. Electron.* 29 (2018) 14232–14238.

[8] J. Navas, C. Fernández-Lorenzo, T. Aguilar, R. Alcántara, J. Martín-Calleja, *Phys. Status*

*Solidi* 209 (2012) 378–385.

[9] T. Sreethawong, S. Laehsalee, S. Chavadej, *Int. J. Hydrogen Energy* 33 (2008) 5947–5957.

[10] R. Dholam, N. Patel, M. Adami, A. Miotello, *Int. J. Hydrogen Energy* 34 (2009) 5337–5346.

[11] A.P. Singh, S. Kumari, R. Shrivastav, S. Dass, V.R. Satsangi, *Int. J. Hydrogen Energy* 33 (2008) 5363–5368.

[12] B. Zhou, M. Schulz, H.Y. Lin, S.I. Shah, J. Qu, C.P. Huang, *Appl. Catal. B Environ.* 92 (2009) 41–49.

[13] E. Barea, X. Xu, V. González-Pedro, T. Ripollés-Sanchis, F. Fabregat-Santiago, J. Bisquert, *Energy Environ. Sci.* 4 (2011) 3414.

[14] M. Long, P. Hu, H. Wu, Y. Chen, B. Tan, W. Cai, *J. Mater. Chem. A* 3 (2015) 5592–5598.

[15] W.W. Lee, C.S. Lu, C.W. Chuang, Y.J. Chen, J.Y. Fu, C.W. Siao, C.C. Chen, *RSC Adv.* 5 (2015) 23450–23463.

[16] J. Yang, L. Xu, C. Liu, T. Xie, *Appl. Surf. Sci.* 319 (2014) 265–271.

[17] S. Sun, W. Wang, L. Zhang, L. Zhou, W. Yin, M. Shang, *Environ. Sci. Technol.* 43 (2009) 2005–2010.

[18] C. Liu, X.J. Wang, *Dalt. Trans.* 45 (2016) 7720–7727.

[19] H. Wang, L. Xu, C. Liu, Y. Lu, Q. Feng, T. Wu, R. Wang, *Nanomaterials* 9 (2019) 118.

[20] M. Cui, J. Yu, H. Lin, Y. Wu, L. Zhao, Y. He, *Appl. Surf. Sci.* 387 (2016) 912–920.

[21] M.J.J. Fatima, C. V. Niveditha, S. Sindhu, *AIP Conf. Proc.* 2082 (2019).

[22] M.J. Jabeen Fatima, C. V. Niveditha, S. Sindhu, *RSC Adv.* 5 (2015) 78299–78305.

[23] M. Chang, H. Hu, Y. Zhang, D. Chen, L. Wu, X. Li, *Nanomaterials* 7 (2017) 104.

[24] J.F. Porter, Y.G. Li, C.K. Chan, *J. Mater. Sci.* 34 (1999) 1523–1531.

[25] J.I. Peña-Flores, A.F. Palomec-Garfias, C. Márquez-Beltrán, E. Sánchez-Mora, E. Gómez-Barojas, F. Pérez-Rodríguez, *Nanoscale Res. Lett.* 9 (2014) 499.

[26] R. Kamble, S. Mahajan, V. Puri, H. Shinde, K. Garadkar, *Mater. Sci. Res. India* 15 (2018) 197–208.

[27] J. Zhang, M. Li, Z. Feng, J. Chen, C. Li, *J. Phys. Chem. B* 110 (2006) 927–935.

[28] F.D. Hardcastle, I.E. Wachs, *J. Solid State Chem.* 97 (1992) 319–331.

[29] X. Jiang, Y. Ma, C. Zhao, Y. Chen, M. Cui, J. Yu, Y. Wu, Y. He, *J. Mater. Res.* 33 (2018)

2385–2395.

[30] C. Liang, C.G. Niu, L. Zhang, X.J. Wen, S.F. Yang, H. Guo, G.M. Zeng, *J. Hazard. Mater.* 361 (2019) 245–258.

[31] A.A. Putri, S. Kato, N. Kishi, T. Soga, *J. Sci. Adv. Mater. Devices* 4 (2019) 116–124.

[32] X. Liu, R. Yi, N. Zhang, R. Shi, X. Li, G. Qiu, *Chem. – An Asian J.* 3 (2008) 732–738.

[33] H. Cheng, B. Huang, Y. Dai, X. Qin, X. Zhang, *Langmuir* 26 (2010) 6618–6624.

[34] Z.-S. Wang, Y. Cui, K. Hara, Y. Dan-oh, C. Kasada, A. Shinpo, *Adv. Mater.* 19 (2007) 1138–1141.

[35] S. Hore, C. Vetter, R. Kern, H. Smit, A. Hinsch, *Sol. Energy Mater. Sol. Cells* 90 (2006) 1176–1188.

[36] C.-S. Chou, M.-G. Guo, K.-H. Liu, Y.-S. Chen, *Appl. Energy* 92 (2012) 224–233.

[37] S.A.M. Samsuri, M.Y.A. Rahman, A.A. Umar, M.M. Salleh, *Ionics (Kiel).* 23 (2017) 3533–3544.

[38] A.A. Putri, S. Kato, N. Kishi, T. Soga, *Jpn. J. Appl. Phys.* 58 (2019) SAAD09.

[39] S. Sfaelou, D. Raptis, V. Dracopoulos, P. Lianos, *RSC Adv.* 5 (2015) 95813–95816.

# CHAPTER 7

# CONCLUSION

## 7.1. Overall conclusion

This thesis described the synthesis and deposition of bismuth oxyiodide (BiOI) by several methods onto the FTO glass substrates. Also, it showed the possibility to use other bismuth-based materials for solar cell application. The properties of BiOI and other materials were discussed and the performance in the solar cells was also studied. In the general conclusion, it could be highlighted that the way in the synthesis of BiOI could result in the different property of BiOI which had the consequence on the different photovoltaic performance of BiOI.

First, from the modified SILAR treatment, the work showed the obtained BiOI which was confirmed by the XRD and Raman analysis. SEM characterization showed the flaky BiOI like it is shown in the previous work by some researchers. Due to the different angle during the dip-coating process in a modified SILAR, it could result in the different properties of BiOI films. The tilting substrate also allowed the thickening films. Therefore, the changing in the FTO substrate orientation could effect on the optical properties, crystallinity, size, and morphology of BiOI films. The thicker film of BiOI has the longer absorption in the visible spectral range. However the thinner film from perpendicular substrate had the best performance with the Jsc and Voc up to 1.47 $mA/cm^2$ and 0.465 V in the BiOI solar cell structure.

Second, by using the different concentration in the synthesis of BiOI, it resulted in the different properties of BiOI films. Precursor concentration could direct the BiOI growth which was shown by the increase in the solar cell performance of BiOI cell up to the concentration of 7 mM and the performance decreased due to the prepared solutions from 8 up to 10 mM. The maximum Jsc was 2.2 $mA/cm^2$. From the analysis, it can be noticed that the higher concentration

of $Bi(NO_3)_3$ and KI induced the growth of the bigger flaky and rod-like BiOI which reduced the solar cell performance due to the overdeposition of BiOI in the higher concentration.

Another way has been developed for the first time to prepare BiOI films, namely spin-SILAR. This method can be proposed to be developed for synthesis BiOI in the future as it consumes the lesser time than the conventional SILAR. The less remained waste also can be a beneficial thing through this method. Spin-SILAR is able to result in the BiOI which was confirmed by XRD and Raman analysis. The good quality of BiOI film also could be obtained by spin-coating process although the washing step was eliminated. To sum up, the SILAR process assisted with the spin-coating can be an alternative way to produce BiOI films, whereas the number of reaction cycle in SILAR is also being an important parameter for controlling the properties of BiOI. However, the resulted performance was not higher as the previous work. It only achieved the best solar cell parameter of 612 $\mu A/cm^2$; 0.446 V; and 0.103 % for its Jsc, Voc, and PCE, respectively.

Next, BiOI films could be prepared by deposition of BiOI powder via doctor blade method. However, the morphology of resulted BiOI was totally different from the previous resulted BiOI by a modified SILAR. The sheet-like materials have just existed instead of the flaky materials although its crystal pattern was in line with the JCPDS data of BiOI and previous research by some researchers. Annealing treatment on this BiOI also has the effect on the chemical and physical properties, also its photovoltaic activity. It could result in the oxygen-abundant and iodine-deficient bismuth materials from the parent BiOI. The structure, morphology, and its optical properties of BiOI films were changed. Due to the annealing at 300, 450, and 550 $^oC$, it allowed the transformation from BiOI to $Bi_7O_9I_3$, $Bi_5O_7I$, and $\beta$-$Bi_2O_3$. The heated material at 300 $^oC$ might be $Bi_7O_9I_3$ which had the best photovoltaic cell performance in comparison to other materials.

Besides BiOI, the derivation of this bismuth oxyhalide material like $Bi_5O_7I$ could be applied as the composite material in the $Bi_5O_7I/TiO_2$ composite films. Since from the previous work it could be noticed that the annealing could convert the BiOI to the different ratio of Bi:O:I materials, $Bi_5O_7I/TiO_2$ can be prepared by annealing of $BiOI/TiO_2$ films at 450 $^oC$. These materials could be utilized as the photoanode in DSSC. A ratio 1:4 for $Bi_5O_7I:TiO_2$ reached the best efficiency among the DSSC photovoltaic devices, which up to 1.9% and 0.083% for 100% for $Bi_5O_7I$ without using the dye.

## 7.2. Suggestion for the future work

BiOI is the promising semiconductor for photocatalysis and photovoltaic application. However, the solar cell performance in this work is low. Therefore, it needs an improvement for the BiOI solar cell performance. The prepared BiOI films with the thin layer and having the good performance in the visible spectral range are needed. The synthesis of BiOI directly from the solid raw material may be attempted to obtain the thin BiOI films which have the broader absorption in the visible spectral range and controllable morphology.

Second, finding the materials which have the longer absorption in the visible light and mixing it with the BiOI may result in the longer visible absorption. If the longer absorption of BiOI material can be obtained, the solar cell performance may be better. Moreover, the choosing of appropriate electrode is also important in this research field. Suitable hole and electron transport layer can be attempted also to construct the BiOI solar cell in order to get the better performance in the BiOI photovoltaic device. Moreover, the optimization of synthesized BiOI by spin-SILAR can be an effort to get the better properties of denser BiOI for photovoltaic application. Last, studying more for the defect property of BiOI also can be proposed to gain the better understanding in the BiOI application for solar cell.

## Acknowledgment

I am grateful to Allah Almighty for giving me a chance to study PhD in Nagoya Institute of Technology (NITech), guiding me to finish this program and tackling the toughest of problems. There is no ease except that which He makes easy. My appreciation is also goes to the Government of The Republic of Indonesia for the financial support during the PhD program through Ministry of Religious Affairs (MORA) Scholarship.

I would like to express my gratitude to my supervisor, Prof. Tetsuo Soga from Department of Electrical and Mechanical Engineering NITech for giving me the opportunity to study and work for PhD program under his supervision, for the patient guidance, encouragement, and advice he has provided throughout my time as his student. I also express my gratitude to Dr. Naoki Kishi, Associate Professor and Dr. Shinya Kato, Assistant Professor from Department of Electrical and Mechanical Engineering NITech for the kind support, valuable guidance, suggestion, and nice discussion during this PhD journey. I also would like to thank the committee member of Department of Electrical and Mechanical Engineering, Nagoya Institute of Technology, Dr. Masashi Kato, Associate Professor for giving the valuable comments and suggestions to improve my thesis.

Special thanks go to my beloved husband, mother, and sisters for their prayers, motivations, and patience. Also the special prayer for my father *yarhamhu*, may Allah grant him in Jannah. *Jazaakumullaahu khairan katsiran*.

Last, I thank Soga-Kishi-Kato laboratory members and staff at NITech, also all of friends in Nagoya, for helping me during studying and living in Japan.

## List of publication

List of paper publication

1. Angle dependence of synthesized BiOI prepared by dip coating and its effect on the photovoltaic performance
   Anissa A. Putri, Shinya Kato, Naoki Kishi and Tetsuo Soga
   *Japanese Journal of Applied Physic, December 2018,* ***Jpn. J. Appl. Phys. 2019, 58, SAAD09***
2. Relevance of precursor molarity in the prepared bismuth oxyiodide films by successive ionic layer adsorption and reaction for solar cell application
   Anissa A. Putri, Shinya Kato, Naoki Kishi and Tetsuo Soga
   *Journal of Science: Advanced Materials and Devices, March 2019,* ***J. Sci. Adv. Mater. Devices 2019, 4, 116–124***
3. Study of annealing temperature effect on the photovoltaic performance of BiOI-based materials
   Anissa A. Putri, Shinya Kato, Naoki Kishi and Tetsuo Soga
   *Applied Sciences, August 2019,* ***Appl. Sci. 2019, 9(16), 3342***
4. $TiO_2/Bi_5O_7I$ nanocomposite for photoanode of electrochemical cell
   Anissa A. Putri, Shinya Kato, Naoki Kishi and Tetsuo Soga
   *Experimental and Theoretical Nanotechnology, September 2019,* ***Exp. Theo. NANOTECHNOLOGY 3 (2019), 61– 70***
5. $TiO_2/Bi_5O_7I$ composite films for dye-sensitized solar cells
   Anissa A. Putri, Shinya Kato, Naoki Kishi and Tetsuo Soga
   *Journal of Electronic Materials, December 2019,* ***Journal of Elec Materi (2019)***
6. A simple spin-assisted SILAR of BiOI films preparation for photovoltaic application
   Anissa A. Putri, A. A. Abuelwafa, Shinya Kato, Naoki Kishi, Tetsuo Soga
   *SN Applied Sciences, December 2019,* ***SN Appl. Sci. 2, 119 (2020)***

List of international conference presentation

1. Properties of BiOI Films Synthesized by the Annealing of $BiI_3$ in the Air
   Anissa A. Putri, S. Kato, N. Kishi, T. Soga
   *International Conference on Nanomaterials- Research & Application, NANOCON 2019, Brno Czech Republic, October 2019*
2. Application of $TiO_2/Bi_xO_yI_z$ composite for photoanode in the photoelectric cell
   Anissa A. Putri, S. Kato, N. Kishi, T. Soga
   *International Conference on Multifunctional, Hybrid and Nanomaterials, Sitges Spain, March 2019*
3. Effect of $Bi_5O_7I$ addition to the $TiO_2$/BiOI composite films on the dye-sensitized photovoltaic cells performance
   Anissa A. Putri, S. Kato, N. Kishi, T. Soga
   *International Conference on Multifunctional, Hybrid and Nanomaterials, Sitges Spain, March 2019*
4. Effect of molar concentration on the morphological, structural and optical properties of BiOI films
   Anissa A. Putri, S. Kato, N. Kishi, T. Soga
   *Japan-Korea Joint Student Seminar, Nagoya Japan, February 2019*
5. Molar concentration precursor effect on the optical and photovoltaic properties of BiOI films prepared by SILAR
   Anissa A. Putri, S. Kato, N. Kishi, T. Soga
   *International Symposium on Optobiotechnology, Nagoya Japan, February 2019*
6. Angle dependence in the synthesis of BiOI film via dip coating method
   Anissa A. Putri, S. Kato, N. Kishi, T. Soga
   *10th International Symposium on Advanced Plasma Science and its Applications for Nitrides and Nanomaterials (ISPlasma), Nagoya Japan, March 2018*

List of national conference presentation

1. One-pot solvent free synthesis of BiOI films via oxidation of $BiI_3$ in air
   Anissa A. Putri, A. A. Abuelwafa, S. Kato, N. Kishi, T. Soga
   *JSAP Autumn Meeting 2019, Hokkaido Japan, September 2019*

2. Annealing Treatment of $TiO_2$/BiOI Heterostructure: Effect on its Photovoltaic Performance
   Anissa A. Putri, S. Kato, N. Kishi, T. Soga
   *JSAP Autumn Meeting 2018, Nagoya Japan, September 2018*